QATAR UNIVERSITY

COLLEGE OF ENGINEERING

EXPERIMENTAL INVESTIGATIONS AND COMPUTATIONAL FLUID DYNAMIC PREDICTIONS OF PRESSURE DROP CHARACTERISTICS IN MULTIPHASE FLOW FOR CONCENTRIC INCLINED ANNULI IN NEAR HORIZONTAL WELLS

BY

MOTASEM WADI NASRALLA ABDELRAZEQ

A Thesis Submitted to

the College of Engineering

in Partial Fulfillment of the Requirements for the Degree of

Masters of Science in Mechanical Engineering

June 2022

COMMITTEE PAGE

The members of the Committee approve the Thesis of
Motasem Abdelrazeq defended on 17/05/2022.

Prof. Ahmad K.Sleiti
Thesis/Dissertation Supervisor

Prof. Mohammed Al-Khawaja
Committee Member

Prof. Samer Ahmed
Committee Member

Prof. Abu Rashid Hasan
Committee Member

Dr. John-John Cabibihan
Committee Member

Approved:

Khalid Kamal Naji**,** Dean, College of Engineering

ABSTRACT

Abdelrazeq, Motasem Wadi Nasralla, Master: June 2022,

Masters of Science in Mechanical Engineering

Title: Experimental Investigations and Computational Fluid Dynamic Predictions of Pressure Drop Characteristics in Multiphase Flow for Concentric Inclined Annuli in Near Horizontal Wells

Supervisor of Thesis: Ahmad K. Sleiti.

In oil and gas sectors, the accuracy of pressure drop predictions plays significant role in designing multiphase flow systems. In recent decades, there is a considerable amount of theoretical and experimental studies dealing with pressure drop predictions for multiphase flow using the hydraulic diameter concept for non-circular cross-section pipes and annular geometries. In single-phase flow applications, applying the hydraulic diameter has been proven to be accurate enough. However, the accuracy of using the hydraulic diameter in multiphase flow systems for annular geometries is questionable and poorly describes the characteristics of the annular flow, which is a research gap that needs to be addressed properly. Recently, the computational modelling has become a significant tool that has proven its reliability in solving and analyzing the dynamics of the fluids and complex multiphase problems. Therefore, in this thesis multiple single- and two-phase flow experiments were conducted at Texas A&M University at Qatar to study the pressure characteristics of liquid-air phase flow in a concentric annulus under different inclination angles to evaluate and judge the theoretical correlations. Then, a computational fluid dynamic model has been developed to simulate a coupled transient two-phase flow using ANSYS software. Two different combinations of liquid-air phase have been experimented using two different liquids (water and Flowzan), the fluids are

flowing in an annular pipe with inner and outer diameters of 6.35 cm, and 11.43 cm, respectively, liquid flow rate range from 192 to 315 kg/min and gas injection pressure range from 1 to 2 bar.

Repeatability test showed that the closeness of agreement between the results of successive measurements is as high as $\cong 98.64\%$. The implementation of the hydraulic diameter concept in single phase flow showed satisfactory results with a maximum error of 3.9%. However, in two-phase flow, a remarkable difference of about 30% to 81% was observed between the actual and predicted pressure drop values using theoretical two-phase flow correlations. Compared with other theoretical approaches, Beggs and Brill correlation performs the best by predicting the results in the error range of $\pm 40\%$.

ANSYS 2021 was used to develop a two-phase computational fluid dynamics (CFD) model using Eulerian-Eulerian as the multiphase flow model and shear stress transport (SST) as the turbulence model. The CFD results were validated using the conducted in this thesis experimental results. The developed CFD model successfully predicted the experimental pressure drop data with an error in the range of $\pm 10\%$ with an absolute average relative error of 8.4%. The experimental and CFD results and approach developed in this thesis serves as a reference for future research to accurately predict the pressure drop for two-phase flow in annular and other complex geometries.

DEDICATION

I dedicate my thesis work to my family and my friends for their marvelous support and encouragement throughout the research.

ACKNOWLEDGMENTS

This thesis was made possible by an Award from Qatar National Research Fund (a member of Qatar Foundation) [GSRA7-2-0427-20027]. I would like to acknowledge the support of Qatar University for providing all the needs to achieve the requirements of this study.

I would like to express my sincere gratitude and appreciation to my supervisor Prof. Ahmad Sleiti for his continuous support and direct supervision in my thesis, and his guidance and patience throughout the project. Also, I would like to acknowledge Dr. Mohammad Rahman who helped me with designing the experiments in TAMUQ. This project would not have been done without the help and valuable knowledge they have provided me with.

TABLE OF CONTENTS

DEDICATION v

ACKNOWLEDGMENTS vi

LIST OF TABLES xi

LIST OF FIGURES xii

Chapter 1: Introduction 1

1.1 Background 1

1.2 Fluid Flow Through Annular Cross-Sections 3

1.3 Aim and Objectives 4

1.4 Motivation 5

1.5 Thesis Layout 6

Chapter 2: Literature Review 8

2.1 Two-Phase Flow 8

2.2 Annular Tubes 17

2.3 Two-phase Computational Fluid Dynamic Models 19

Chapter 3: Methodology 22

3.1 Experimental Work 22

3.1.1 Water-Air Experimental Procedure and Data Collection 23

3.1.2 Flowzan-Air Experimental Procedure and Data Collection 25

3.1.3 Safety Concerns of the Test Setup 25

3.1.4 Materials and Operational Conditions 26

3.2 Flow Loop Equipment and Main Components 27
3.2.1 Frame 27
3.2.2 Flange 29
3.2.3 Pump 30
3.2.4 Flow Meter Sensors 31
3.2.5 Electrical Cabinet 33
3.2.6 Programmable Logic Controller 34
3.2.7 Electro-Pneumatic Regulator 34
3.2.8 Motors 34
3.2.9 Hydro cyclone 35
3.2.10 Tank 36
3.2.11 Gas Injection Device 37
3.3 Theoretical Models 40
3.3.1 Basic Parameters in Multiphase Flow 40
3.3.2 Homogenous Model 41
3.3.3 Separated Flow Model 43
3.3.4 Beggs and Brill Correlation 44
3.4 Development of the Computation Fluid Dynamic Model 49
3.4.1 Geometry 49
3.4.2 Meshing 50
3.4.3 Setting Up the Model 52

Chapter 4: Results and Discussion 53
4.1 Calibration of the Dynamic Pressure Sensors 53
4.2 Single Phase Flow 54
4.2.1 Repeatability Test 54
4.2.2 Experimental Pressure Drop Measurements 55
4.2.3 Theoretical Model 56
4.3 Two-Phase Flow (Water-Air) 57
4.3.1 Water-Air Experiments 58
4.3.2 Theoretical Correlations 60
4.4 Two-Phase Flow (Flowzan-Air) 71
4.5 Correlation development 75
4.6 Computational Fluid Dynamics 77
4.6.1 Multiphase Model 77
4.6.2 Turbulence Model 78
4.6.3 Validation of the Developed Model 80
4.6.4 Model Comparison with Theoretical Models 81
Chapter 5: Conclusions and Future Work 83
5.1 Conclusions 83
5.2 Recommendations for Future Work 85
References 86
Appendix A: Nomenclature 94

Appendix B: One-Phase Liquid Experiments.....96

Appendix C: Two-Phase Gas-Liquid Experiments.....99

LIST OF TABLES

Table 1: Various Viscosity Correlations for Homogeneous Models 13

Table 2: Literature Studies on Various Computational Fluid Dynamic Models 21

Table 3: Operational Conditions for Single and Two-Phase Flow Experiments.....26

Table 4: Specifications of the dynamic pressure sensor 39

Table 5: Operational Conditions for the Repeatability Test 55

Table 6: Operational Conditions.....56

Table 7: Two-Phase Operational Conditions.....58

Table 8: Constants of the developed correlations.....76

Table 9: Range of applicability.....76

Table 10: Nomenclature.....94

Table 11: Single Phase Experiments Using Water at 0 Degrees 96

Table 12: Single Phase Experiments Using Water at 5 Degrees 96

Table 13: Single Phase Experiments Using Water at 8 Degrees 97

Table 14: Single Phase Experiments Using Flowzan at 0 Degrees 97

Table 15: Single Phase Experiments Using Flowzan at 5 Degrees 98

Table 16: Single Phase Experiments Using Flowzan at 8 Degrees 98

Table 17: Two Phase Experiments Using Water-Air at 0 Degrees 99

Table 18: Two Phase Experiments Using Water-Air at 5 Degrees 100

Table 19: Two Phase Experiments Using Water-Air at 8 Degrees 101

Table 20:Two Phase Experiments Using Flowzan-Air at 0 Degrees 102

Table 21: Two Phase Experiments Using Flowzan-Air at 5 Degrees 103

Table 22: Two Phase Experiments Using Flowzan-Air at 8 Degrees 104

LIST OF FIGURES

Figure 1: Two-phase possible combinations....2
Figure 2: The most used energy sources [3]....3
Figure 3: Consequences of unaccurate pressure drop predictions....6
Figure 4: Flow regimes for two-phase flow [16]....9
Figure 5: Main components of TAMUQ flow loop system....23
Figure 6: The frame of the flow loop system....27
Figure 7: Schematic drawing of the frame....28
Figure 8: Manual concentricity adjuster....28
Figure 9: Flanges attached to the tank....29
Figure 10: Flanges connect the main pipe together....30
Figure 11: Slurry pump....31
Figure 12: Gas flow meter....32
Figure 13: Electrical cabinet....33
Figure 14: Hydrocyclone device....35
Figure 15: Main tank....36
Figure 16: Small mixing tank....37
Figure 17: Air injection system....38
Figure 18: Injection tubes....38
Figure 19: Dynamic pressure sensor....39
Figure 20: Separated phases [74]....43
Figure 21: CAD geometry....50
Figure 22: CAD meshing, isometric view....51
Figure 23: CAD meshing, side view....51
Figure 24: Calibration of dynamic pressure sensors....53

Figure 25: Repeatability test of the experimental pressure drop for two experiments 54

Figure 26: Validation of the experimental results.....57

Figure 27: Experimental pressure drop at 0, 5, and 8 degrees of inclination for a range of water flow rate and inlet air pressure.....60

Figure 28: Comparing the experimental pressure drop data with Dukler's and Shannak's homogenous theoretical models at 0, 5, and 8 degrees with gas injection pressure of 1, 1.5 and 2 bars. 64

Figure 29: Comparing the experimental pressure drop data with Lockhart-Martinelli's separated model at 0, 5, and 8 degrees with gas injection pressure of 1, 1.5 and 2 bars. 67

Figure 30: Comparing the experimental pressure drop data with Beggs and Brill theoretical model at 0, 5, and 8 degrees with gas injection pressure of 1, 1.5 and 2 bars. 70

Figure 31: Comparing the experimental pressure drop data for Flowzan-Air two-phase flow with theoretical models at 0, 5, and 8 degrees with gas injection pressure of 1, 1.5 and 2 bars. 74

Figure 32: The range of error between the experimental data and the developed model 76

Figure 33: Validation of the computational model for Water-Air and Flowzan-Air experiments at 0, 5, and 8 degrees with gas injection pressure of 1, 1.5 and 2 bars....80

Figure 34: Comparison between different pressure models using Water-Air and Flowzan-Air combinations at 0, 5, and 8 degrees with gas injection pressure of 1, 1.5 and 2 bars. 82

CHAPTER 1: INTRODUCTION

Multiphase flow in fluid dynamics is described as the simultaneous flow of substances comprising more than one phase of thermodynamic phases [1]. The phases could consist of water, oil, solid particles or gas. Recently, considerable attention has been given to multiphase flow systems due to their applicability in variety of fields. In this chapter, a background study related to two-phase flow will be provided including its dynamic behavior and properties together with a brief presentation of two-phase flow with annular geometries and its significance to oil and gas industries. After that, the motivation along with the aim and objectives of the study will be stated. Finally, the overall thesis sections including a description of each chapter will be given.

1.1 Background

Two-phase flow is a complex physical phenomenon where two interactive distinct phases with common interfaces occurs through a channel. Two-phase flows are being used in various worldwide industries for several purposes, such as, petroleum industries, power plants, mining plants, biomedical and pipeline engineering. Two-phase flow can occur in a single or multicomponent system. There are several possible combinations for multiphase flow, Figure 1 presents the most common phases, which are: liquid-gas, liquid-solid, solid-gas, and liquid-liquid. The liquid-gas type is considered to be one of the most complex flows among the aforementioned types, because these flows combine both of the deformable interface characteristics and the compressibility attributes. [1-2].

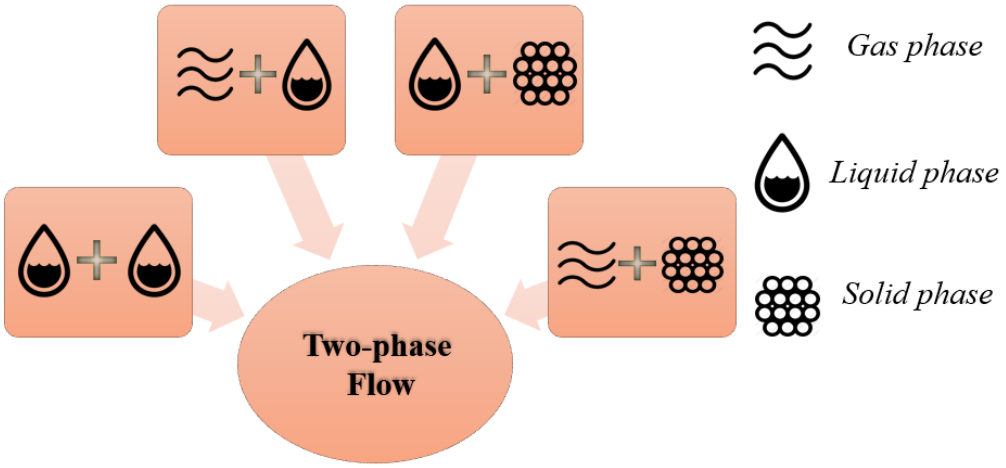

Figure 1: Two-phase possible combinations

Multiphase flow systems in the oil and gas industry, in particular, have many applications that need to be understood and predicted accurately. Fossil fuels, for example, (such as coal, oil, and natural gas) are of great importance and widely used in various industries and applications, as they are playing a dominant role in global energy systems, and they are considered to be the driver of the economic growth. According to the U.S Energy Information Administration (EIA), the natural gas is one of the most consumed energy sources. This is clearly illustrated in Figure 2, where the natural gas is considered to be the most energy source that is being used for electricity generation, reaching around 4,000 billion kilowatt-hours annually [3]. The natural gas provides the base ingredients for numerous products in industries, such as: plastic, fabrics, and fertilizer, not to mention its manufacturing applications represented in glass melting, metal preheating, waste treatment, food processing, and petroleum refining, in addition to that, it is being used in some residential and commercial applications like heating, ventilation and air conditioning (HVAC) systems.

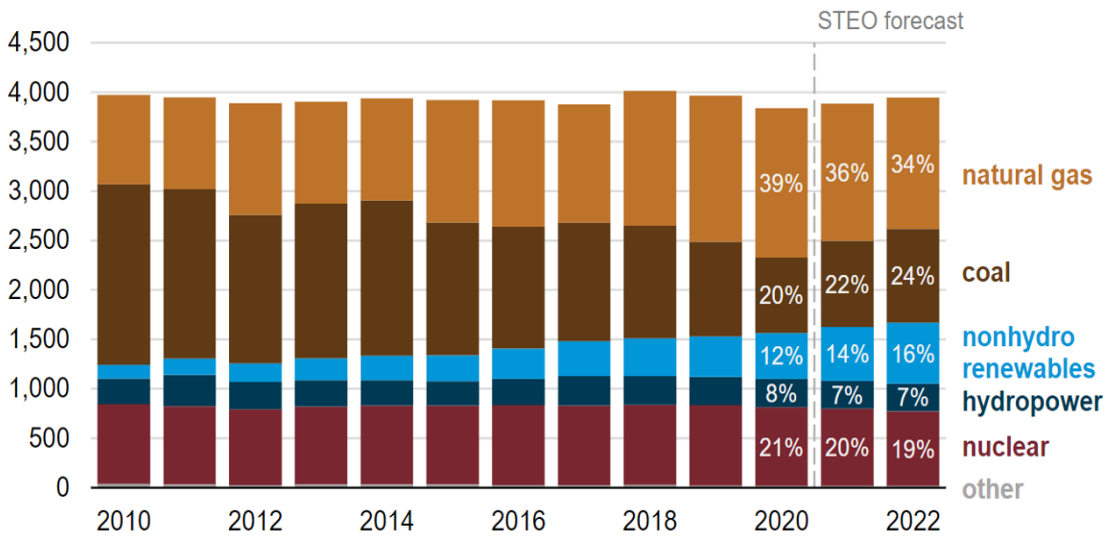

Figure 2: The most used energy sources [3]

One of the major parameters that the oil and gas industries are investigating in their operations is the frictional pressure drop, and that is due to the fact that pressure drop has a decisive role in the flowline in cases where the flowline is long, and when the diameter is small [4]. The majority of oil wells eventually produce both oil and gas from the formation as well as water in some cases. Two phase flow is therefore prevalent in oil and gas wells. The pressure drop and accompanying flow rates of the fluids are commonly used to study multiphase flow in pipelines. Estimating the pressure drop is difficult because of the diverse hydrodynamics and turbulence characteristics, which is significantly different from the case of single-phase flow. Therefore, under- or over-estimating the pressure drop in the natural gas or oil exploration processes, will negatively affect the productivity and the economic growth.

1.2 Fluid Flow Through Annular Cross-Sections

In oil and gas industries, multiphase flow in annular conduits can occur under a number of operational settings [5]. The following is a list of cases in which fluid flow via

annular cross-sections is required:

1) In wells where using the production tubing is extremely difficult and restrictive owing to the high frictional losses. This is often appearing in wells with high reservoir pressure forces.
2) When a reduction in the flow area and increasing in fluid velocity is desired in order to prevent liquid accumulation at the well's bottom, which might in some cases result in a decrease or total stoppage of liquid and/or gas production.
3) In dual wells, where it is needed to deliver the upper and lower zones up the external annulus and production tubing.
4) In sucker rod pumping wells, also referred as “beam pumping”, where the liquid and gas travel up the annulus.

1.3 Aim and Objectives

The aim of this study is to investigate the pressure drop characteristics in single- and two-phase flow through annuli using theoretical, experimental, and computational approaches. That will be completed through the following:

1) Gathering of data by conducting some experiments in a multiphase flow loop system at Texas A&M University at Qatar.
2) Thoroughly studying the effect of the liquid flow rate, the gas injection pressure and inclination angle on the pressure losses in single and two-phase flows through annular pipelines.
3) Using appropriate empirical correlations with momentum and energy balance equations to accurately develop, model, and simulate a coupled transient two-phase flow using ANSYS software.

4) Assessing and judging the available correlations and theoretical models by comparing them with the actual pressure drop data obtained from annular geometry.
5) Developing and validating computational fluid dynamics (CFD) model that can accurately predict the pressure drop in two-phase gas-liquid flow in annular cross-section.

1.4 Motivation

Multiphase flow in pipelines or annuli is of great importance and broadly used in several industries and various applications. In the industrial sector, more attention has been given to the well drilling operation to fulfill the extreme high demand of natural gas. The severity of under or over-estimation of pressure drop is evident in oil and gas industries, especially at extreme conditions associated with unbalanced operation [6-7]. Failing in predicting the pressure drop in these situations may cause dramatic blowouts with very serious consequences, including financial losses, damaging the environment, and loss of personnel's lives [8]. As illustrated in Figure 3, these consequences negatively impact various sectors in the society, such as: financial, healthcare, and environmental sectors. And a good example of that is the blowout that happened back in 2010 in Macondo. The financial and environmental consequences of this blowout were massive, as it has lasted almost three months and wasted around 172 million gallons of oil at a depth of about 1500 meters [6]. Therefore, in such cases, accurate estimation of pressure drop is essentially needed for timely response and well control measures.

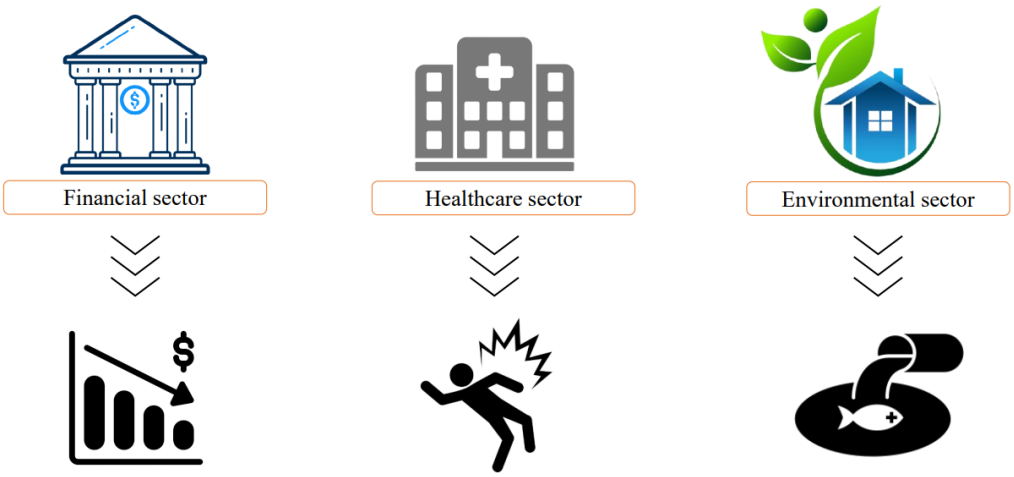

Figure 3: Consequences of unaccurate pressure drop predictions

1.5 Thesis Layout

In Chapter 2, a literature review will be completed containing all aspects of two-phase flow including circular and annular geometries together with the available theoretical correlations for pressure drop predictions. More attention will be given to the annular cross-sectional tubes which is the main focus of this study. Comprehensive review of some computational fluid dynamic models will be addressed and evaluated in many areas, including the multiphase model, turbulence model, and the optimized discretization methods to investigate the accuracy and confirm the convergence in the governing equations.

In Chapter 3, the methodology of this study will take place including experimental, theoretical and computational work. The section will start describing the experimental work including the properties of the used materials, the experimental procedure for both single- and two-phase flows, detailed explanation of the main components of the flow loop system, in addition to some safety concerns related to the test set-up. Then, an introduction for the computational fluid dynamic model will be stated by introducing

general aspects of model development starting from the geometry, then meshing, all the way to setting up the multiphase model.

Chapter 4 will demonstrate all the obtained experimental results for single- and two-phase flows. The section started with an explanation of dynamic pressure sensor calibration. Then, the repeatability test was performed in order to ensure that the data generated from the system is repeatable. The results of the test set-up will be validated by comparing the experimental results of single-phase flow with a theoretical correlation. Multiple two-phase flow experiments will be demonstrated using Water-Air and Flowzan-Air two-phase combinations. Finally, the theoretical models are to be judged by the implementation of the hydraulic diameter.

In Chapter 5 a conclusive summary will be provided containing the main outcomes of this research. Future directions and recommendations to enhance and improve the sound of the research will also be provided.

CHAPTER 2: LITERATURE REVIEW

In this chapter, a comprehensive literature review will be conducted. The chapter starts with reviewing the differences between the single- and two-phase flows. The chapter demonstrated the available theoretical models that were developed for two-phase flow. Each model has its own applicability, and each one was developed based on different assumptions. More focus has been given to recent studies and experimental investigations that have been conducted on annular geometries. Finally, a review has been made on recent two-phase computational fluid dynamic models along with some investigations on their processing capabilities which are represented in their multiphase and turbulence models.

2.1 Two-Phase Flow

Unlike the single-phase flow, two-phase flow simulates the simultaneous flow of two different fluids with distinct fluid properties and phases. There are several types for two phase flow such as liquid-gas, liquid-solid, solid-gas, and liquid-liquid. The liquid-gas type which is the focus of this study is considered to be one of the most complex flows among the aforementioned types [9-10].

In the single-phase flow, there are many parameters affecting the pressure drop like the shape, size, velocity and properties of the fluid [11]. However, in the two-phase flow there are much more parameters that could affect the flow pattern and pressure drop characteristics like the direction of the fluids, the interference between the fluids, and the configuration of the conduit with its alignment. The two-phase flow configuration is not limited to laminar, transition and turbulence patterns, as there are much more. There are many possible flow patterns or regimes that can be formed in the horizontal

two-phase flow, such as, bubble flow, slug flow, churn flow, annular flow, and wispy annular flow [9-12]. Figure 4 illustrates the flow pattern map for horizontal flow.

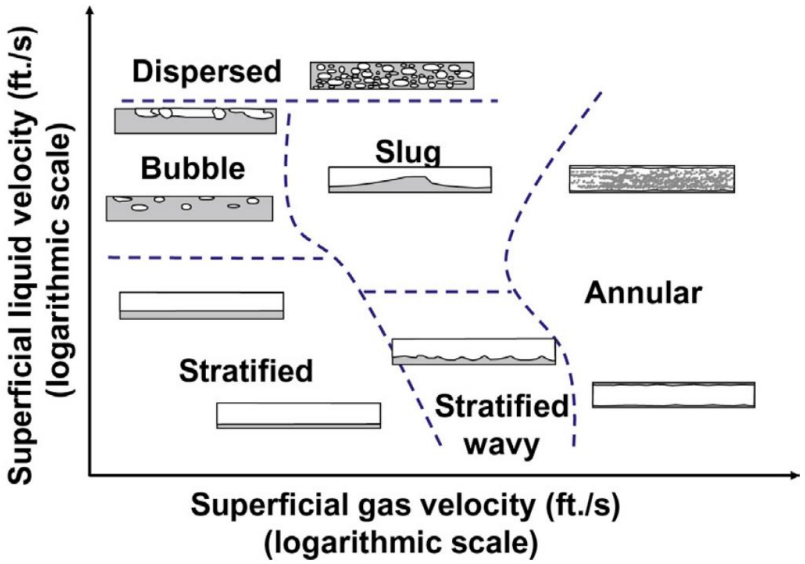

Figure 4: Flow regimes for two-phase flow [16]

Given the complexity of two-phase flow characteristics, some new parameters have been outlined in the following:

The superficial velocity u_s and superficial mixture velocity $u_{s,m}$ of liquid and gas as shown in Equation (1) and Equation (2), are defined as the ratio of the volumetric flowrate over the cross-sectional area of the pipe:

$$u_{s,l/g} = \frac{Q_{l/g}}{A} \tag{1}$$

$$u_{s,m} = \frac{Q_g + Q_l}{A} \tag{2}$$

The mass flux G as shown in Equation (3) is also taken into consideration in two-phase flow calculations, which is the summation of liquid and gas densities multiplied with the superficial velocity of each phase:

$$G = \rho_g * u_{s,g} + \rho_l * u_{s,l} \tag{3}$$

Another parameter is the mass quality of gas, it has been proposed specially for the two-phase flow calculations due to the significance of phases fractions and velocities. The mass quality x in Equation (4), is defined by dividing the ratio of the gas mass flow rate over the total mass flow rate for both fluids. Similarly, the volumetric quality β in Equation (5), has been proposed to define the ratio of the gas volumetric flow rate over the total volumetric flow rate for the two phases.

$$x = \frac{\dot{M}_g}{\dot{M}_g + \dot{M}_l} \tag{4}$$

$$\beta = \frac{Q_g}{Q_g + Q_l} \tag{5}$$

Additionally, the Reynolds number can be found using the superficial velocities for each phase, this Reynold number is equivalent to the single phase one. It can be calculated using Equation (6):

$$Re_{s,l/g} = \frac{\rho * u_s * D}{\mu} \tag{6}$$

Several empirical and semi-empirical models have been established, and most of them can be seen as an extension of the single-phase models. These models are more or less accurate in estimating the pressure drop. The homogenous and separated flow models are two different approaches that have been identified to investigate the pressure drop characteristics of the two-phase flow [17-18].

In the homogeneous flow model, the two-phase flow will be treated as a single phase with a unique single pseudo-fluid estimated as suitable intercorrelations between the properties of liquid and gas phases [19-20]. To estimate the frictional factor using the homogeneous approach, one must find the homogenous Reynolds number using Equation (7).

$$Re_{hom} = \frac{G * D}{\mu_{hom}} \tag{7}$$

The early work started with Wallis in 1969, where he presented a complete mechanistic model that can calculate the liquid hold up and pressure drop in two-phase flow. Wallis' model assumed that the void fraction is equal to the liquid hold up in order to obtain the averaged physical properties [21]. The single-phase pressure drop shown in Equation (8), was used to derive the frictional pressure drop for two phase flow in Wallis model.

Estimation of pressure drop for the single-phase flow:

$$\Delta p = f.\frac{l}{D}.\frac{\rho * \overline{u}^2}{2} \tag{8}$$

Estimation of pressure drop for the homogenous two-phase flow:

$$\Delta p = f.\frac{l}{D}.\frac{G^2}{2 * \rho} \quad (9)$$

A variety of different correlations have been proposed to accurately predict the pressure drop using the homogenous approach. The main parameter that researchers were modifying in their models is the homogenous viscosity. Several studies on the mean two-phase homogenous viscosity have been performed as follows:

McAdams et al. (1942) and Cicchitti et al. (1960) developed expressions that are similar to the two-phase flow density. Dukler et al. (1964a; 1964b) developed an expression using the concept of averaged value of kinematic viscosity. Beattie and Whalley (1982) have proposed an expression taking into consideration some gravity dominant flows. Lin et al. (1991) performed numerous experiments investigating the vaporization of R12 in capillary tubes and based on the results the expression was estimated. Awad and Muzychka (2008) developed an expression based on utilizing the thermal conductivity of porous media. Shannak (2008) proposed another expression by employing the summation of the inertial and viscous forces for each phase [22-29].
Table 1 shows various expressions of the mean two-phase flow viscosity for the homogeneous flow model.

Table 1: Various Viscosity Correlations for Homogeneous Models

Author	Homogeneous models	Reference
McAdams et al. (1942)	$\mu_{hom} = \left(\frac{x}{\mu_g} + \frac{1-x}{\mu_l}\right)^{-1}$	[22]
Cicchitti et al. (1960)	$\mu_{hom} = x * \mu_g + (1-x) * \mu_l$	[23]
Dukler et al. (1964)	$\mu_{hom} = \rho_{hom} * (x * \frac{\mu_g}{\rho_g} + (1-x) * \frac{\mu_l}{\rho_l})$	[24], [25]
Beattie and Whalley (1982)	$\mu_{hom} = \mu_l * (1 - \alpha_{g,hom}) * (1 + 2.5 * \alpha_{g,hom}) + \mu_g * \alpha_{g,hom}$ $\alpha_{g,hom} = \frac{1}{1 + \frac{1-x}{x} * \frac{\rho_g}{\rho_l}}$	[26]
Lin et al. (1991)	$\mu_{hom} = (\mu_l * \mu_g)/\mu_g + x^{1.4}(\mu_l - \mu_g)$	[27]
Awad and Muzychka (2008)	$\mu_{hom} = \mu_l * \frac{2 * \mu_l + \mu_g - 2 * (\mu_l - \mu_g) * x}{2\mu_l + \mu_g + (\mu_l - \mu_g) * x}$	[28]
Shannak (2008)	$\mathrm{Re}_{hom} = \frac{G * D * \left(x^2 + (1-x)^2 * \left(\frac{\rho_g}{\rho_l}\right)\right)}{\mu_g * x + \mu_l(1-x)(\frac{\rho_g}{\rho_l})}$	[29]

In 2012, Xu et al. analyzed the homogenous models and concluded that Beattie and Whalley and McAdams et al. correlations perform the best among the data that was used. They have reported a mean absolute relative error of 40% for most of the homogeneous models except for Cicchitti et al. (1960) whose mean absolute relative error exceeds 55%. In their analysis, Xu et al. used around 3480 data points. However, it is worth mentioning that just around 139 points came from an annular cross-sectional pipe [30].

The separated flow model is another approach to calculate the frictional pressure drop. In this model, the liquid and gas phases are assumed to flow separately in the channel. Each phase will have its own average potential velocity. In this model, the liquid hold up becomes relevant, since the total cross-flow area is occupied by a calculated fraction of gas phase. Lockhart and Martinelli (1949) developed the first separated flow model correlation taking into consideration the frictional multipliers which can be considered as the ratio of the total pressure gradient for both phases to the pressure gradient of each phase flowing separately. The frictional multipliers for liquid and gas, are ϕ_l and ϕ_g, respectively [31-32]. According to Lockhart and Martinelli, the frictional pressure drop of two phase flow for the separated model can be written as follows:

Equation (10) describes the frictional pressure drop for liquid

$$\Delta p_l = f_l . \frac{l}{D} . \frac{[G * (1 - x)]^2}{2 * \rho_l} * \phi_l^2 \tag{10}$$

Equation (11) describes the frictional pressure drop for gas

$$\Delta p_g = f_g . \frac{l}{D} . \frac{[G * x]^2}{2 * \rho_g} * \phi_g^2 \tag{11}$$

The frictional multiplier cannot be obtained from graphs. Thus, several investigations have been performed by Chisholm (1967), Sun and Mishima (2009), and Zhang et al., (2010) to develop a friction factor correlation. Xu et al. (2012) has summarized and analyzed these and other frictional factor correlations. The results showed that the estimation of Sun and Mishima was the most accurate one [33-35].

Equation (12) shows the velocity ratio S, which is another parameter that was developed for the calculation of the separated model. This velocity ration describes the ratio of the gas mass velocity to the liquid mass velocity.

$$S = \frac{u_g}{u_l} \tag{12}$$

Several methods have been proposed to calculate the void fraction (the fraction of the gas phase). The separated flow model void fraction can be calculated using the velocity ration by extending the homogenous void fraction as shown in Equation (13):

$$\alpha = \frac{1}{1 + \frac{1-x}{x} * \frac{\rho_g}{\rho_l} * S} \tag{13}$$

Many other estimations for void fraction have been proposed to calculate the void fraction in this model including the analytical and empirical correlations like Zivi (1964) and Smith (1969), however, Steiner (VDI Heat Atlas, 2010) correlation has proven a good accuracy in estimating the void fraction for the separated model, which is shown in Equation (14) [36-38]. This correlation was derived from the drift flux model of Rouhani and Axelson (1970) [39].

$$\alpha = \frac{x}{\rho_g}\left([1 + 0.12(1-x)]\left(\frac{x}{\rho_g} - \frac{1-x}{\rho_l}\right) + \frac{1.18(1-x)\left[g * \sigma\left(\rho_l - \rho_g\right)\right]^{0.25}}{\dot{m} * sqrt(\rho_l)}\right)^{-1} \tag{14}$$

Beggs and Brill (1973) flow model is another well-known correlation that is being used for pressure drop calculations. The model was developed using the grounds of the homogenous model. This model has a unique calculation procedure in which many variables have to be found before obtaining the pressure drop, including Froud number, the type of the flow pattern, and void fraction/liquid hold-up. Given its applicability to pipes with different inclinations and simplicity, this model is considered to have an acceptable estimation of the characteristics of two-phase flow. However, its accuracy and validity to various pipe geometries and orientations other than the circular pipe is still not proven [40]. In 1990, Whalley has done some investigations and concluded that the homogeneous model gives satisfactory predictions when the density ratio is $\rho l/\rho g < 10$ and the mass flux is $G > 2000$ kg/m²/s [41].

Many studies of two-phase flow through circular tubes have been conducted over the last century. The goal of the research was to fully comprehend the physics of two-phase flow in pipes, both theoretically and experimentally. Bergelin and Gazley (1949) and Kosterin (1949) were among the first to investigate and propose a flow pattern related to the horizontal two-phase flow [42-43]. Following Bergelin, Gazley and Kosterin, several other maps were established by the use of some theoretical estimations or by visual observations in the form of empirical, theoretical or semi-theoretical nature [44-45] .

Additionally, numerous maps have been proposed by conducting several flow pattern experimentations and plotting experimental results [46-51]. The most acceptable flow patterns among the proposed maps are: bubbly flow, plug flow, stratified flow, wavy flow, slug flow and annular flow [52]. However, additional complex hybrid flow

regimes were identified named as subcategorized or combined regimes [53-55].

Recently, numerous investigations have been performed using machine learning classification models to identify the two-phase flow regimes [56-57]. Determining the flow pattern is challenging and needs more investigations because the flow patterns differ by changing the geometry of the pipe, the eccentricity, and the angle of inclination.

2.2 Annular Tubes

In the literature, there are several studies that have been performed for the circular cross-sectional area, but only a limited number of studies have been done towards the two-phase flow in an annular cross section. Salcudean et al. (1983) studied the response of the void fraction and pressure drop after introducing obstructions in the flow. They have concluded that when the obstructions are applied to the flow, the pressure drop is much higher than the case with no obstructions. Furthermore, they have noted that changing the location of the obstruction will change the value of the pressure drop [58-59]. They have observed that the central obstruction has the highest influence on the flow system, and that the available theoretical models lead to inaccurate results and do not simulate the experimental behavior.

Hasan and Kabir (1992) performed several two-phase experiments with different inclinations using annular pipe. They have concluded that at a vertical annular conduit, and just for small ratios of inner to outer diameters, the void fraction of the annular will be close to that of circular geometry [60].

Osamusali (1988) have done multiple experiments using circular and annular geometries. Osamusali noticed that at the same exact conditions the flow regimes do vary from one geometry to another, as there was a shift of the transitions of the flow patterns in the case of annular geometry, and that there is a huge effect of the diameter ratio (inner to outer diameter) through annuli, which is not illustrated in the theoretical models [61-62].

Many other authors like Ekberg et al. (1999), Sunthankar (2003), Wongwises and Pipathatatakul (2006) and Mendes et al. (2011) also compared various annular pipe geometries with circular ones and concluded that there is a discrepancy in the experimental and theoretical results [63]. Ekberg et al. (1999) investigated liquid hold up, flow regimes and pressure drop in their experimental work using horizontal annular concentric pipe [64]. In 2003, Sunthankar have done several experiments using annular pipe, and compared his conclusions with modified pipe flow models and concluded that there is a huge variation [65]. Wongwises and Pipathatatakul (2006) have done multiple experiments using annular concentric two-phase flow system with varying the inclinations. They compared the liquid hold up and pressure drop results with the theoretical models and concluded that there is not a good agreement between the experimental and theoretical results [66].

Applying the hydraulic diameter for single phase flow produced acceptable results, however, applying the definition of the hydraulic diameter in two phase flow is more complicated and studying the mechanics of the flow by adapting it to the annular cross-section is still questionable [67]. Also, the models that were made for the circular cross-section poorly describes the characteristics of the annular flow [67-68]. Overall, as it is

remarked from the previous work, further investigation is still required for annular ducts in horizontal and near horizontals wells. Despite the fact that the concept of hydraulic diameter is still used in the petroleum industry, experimental validation shall be done to ensure that circular pipe flow correlations can be extended to the annular ones. Additional experimental work will be performed at TAMUQ flow loop system and will be compared with the available theoretical models to assess the theoretical models and to fully understand the hydraulics of two-phase flow in annular cross sections.

2.3 Two-phase Computational Fluid Dynamic Models

Recently, the computational fluid dynamics has become a significant tool that solve and analyze mathematical equations by utilizing a certain numerical algorithm. CFD has contributed considerably to many engineering areas such as heat and mass transfer, chemical reactions, fluid flow, etc. Table 2 illustrates various computational dynamic multiphase models

Dhiraj A. Lote et al. (2018) have performed a CFD study using two-phase flow in vertical pipe. The Eulerian-Eulerian multiphase approach with the k−ω shear stress transport (SST) turbulence model were carried out in the calculations. In their study, each phase was considered as interpenetrating continua with the inclusion of the gas phase volume fraction concept [69].

A study has been done by (Shihui et al, 2019) to investigate the gas formation during a gas kick. A volume of fluid (VOF) approach was used as the multiphase model. VOF performs well in this kind of investigations as it has strong processing capabilities of transient and steady state of gas-liquid interface. In their study, the wellbore conditions

were assumed as isothermal, and the gas does not dissolve in the liquid. The governing equations were discretized using the first order upwind scheme, and the surface tension was taken into consideration [70].

Rasel A. Sultan et al. (2019) developed a CFD model by adapting the Eulerian granular approach as the multiphase model. They have run the simulation using various turbulence models. They have concluded that the Reynolds stress model (RSM) worked the best for their model with the least error. First and second up-wind discretization were applied with SIMPLE algorithm to discretize the governing equations. In another work, Rasel A. Sultan et al. have implemented a second CFD model but with Euler–Euler approach, because this time they have applied both of the granular (Fluid-Solid) and non-granular (Fluid-Fluid) fluids [71-72]. Gray and Ormiston (2021) developed a computational inhomogeneous model by using Eulerian multiphase approach. Drag, lift, and wall lubrication forces have also been taken into consideration. They have used two turbulence models which are the SST and k -epsilon. It has been concluded that there was no significant effect of changing the turbulence models [73].

In the present study, ANSYS workbench is used to build a CFD simulation model of a horizontal pipeline The CFD model will be carried out and will be validated using the experimental results of a two-phase flowing through annular cross-section. Eulerian-Eulerian method will be used as the multiphase model. A turbulence model of k−ω shear stress transport (SST) is adopted to analyze multiphase fluid flow. Second order upwind discretization method will be carried out to ensure having an appropriate stability and to accurately confirm convergence in the governing equations.

Table 2: Literature Studies on Various Computational Fluid Dynamic Models

Author	Multiphase Model	Turbulence Model	Phases	Geometry	Pipeline	Reference
Dhiraj A. Lote (2018)	Eulerian–Eulerian approach	k−ω shear stress transport (SST)	Two phase flow (Gas-Liquid)	Circular	Vertical	[69]
Rasel A. Sultan (2019-a)	Eulerian–Eulerian approach	Reynolds stress model (RSM)	Single, two, and three phase flows	Annular	Horizontal	[71]
Rasel A. Sultan (2019-b)	Eulerian-granular approach	Reynolds stress model (RSM)	Single, two, and three phase flows	Annular	Horizontal	[72]
Shihui et al, (2019)	VOF	-	Two phase flow (Gas-Liquid)	Annular	vertical	[70]
Gray and Ormiston (2021)	Eulerian–Eulerian approach	Equation SST and k -epsilon	Two-phase flow (Gas-Liquid)	Circular	Vertical	[73]
Present study	Eulerian–Eulerian approach	k−ω shear stress transport (SST)	Two phase flow (Gas-Liquid)	Annular	Horizontal and near horizontal	-

CHAPTER 3: METHODOLOGY

In this chapter, a detailed description of the experimental setup is provided. Various materials and flow combinations have been used in the experimental work. Several operational conditions have been varied including liquid flow rate, gas injection pressure, and angle of inclination. The procedure of the single- and two-phase experiments are illustrated along with the safety concerns of the test setup. The main equipment and components of the flow loop system with their characteristics are also demonstrated. Several models have been described along with their energy, momentum, and mass equations. Finally, the developed computational dynamic model has been illustrated together with its multiphase and turbulence model.

3.1 Experimental Work

Several experiments were carried out in the horizontal flow loop in Advance Multiphase Flow Assurance and Production Laboratory (AMFAPL) at Texas A&M University at Qatar. The flow loop system has a circular annular geometry which consist of a 6.16 m horizontal two concentric cylinders with an inner and outer diameter of 6.35 cm (2.5 inch), and 11.43 cm (4.5 in), respectively. The outer pipe of the test section is made of transparent acrylic material for ease of observation, whereas the inner pipe is made of Aluminum. The test set up is capable of simulating multiphase flow conditions during drilling and production by varying drilling fluids' viscosities and flow rates. In addition, the system investigates the effect of inclination by adjusting the angle of the system. The main components of the flow loop system are represented in Figure 5.

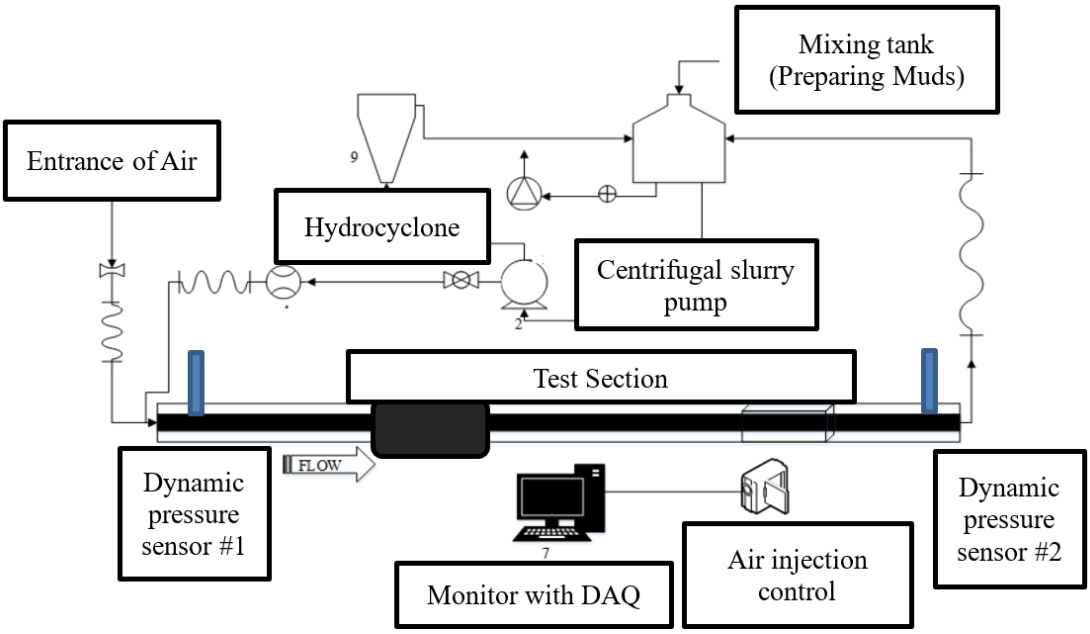

Figure 5: Main components of TAMUQ flow loop system

The frame of the flow loop can reach up to 10 degrees from horizontal. The system is attached to a flow tank with a capacity of 1 m^3 (around 165 gallons) equipped with an agitator, which is a device that is typically used to blend and/or mix various fluids with powders to ensure creating a homogeneous mixture in the tank. The system is connected to data acquisition hardware and sensors that allow monitoring of pressure, temperature and frequency. The air can be injected up to a maximum pressure of 3 bars, while the pump rotational speed can be varied from 0 up to 1200 RPM.

3.1.1 Water-Air Experimental Procedure and Data Collection

1) The hose has been connected to the water line and the water inlet valve has been switched on.
2) The tank has been filled up to 800 liters by the use of the level sensor that is designed to monitor and maintain a certain water level.

If for whatever reason the level exceeded 800 L, the flow switch will immediately

shut the electrically controlled solenoid valve.

3) After reaching the desired amount of water, the water inlet valve has been closed and the hose has been removed.
4) The pump has been started and the liquid entering annulus has been monitored

Also, one should check for leaks. If leak is identified, the emergency shut-off button that is located on the electrical cabinet should be pressed.

5) The desired RPM has been adjusted

The rpm of the pump was increasing gradually to 500 RPM and kept constant for some time to eliminate the existence air bubbles (if any) and to ensure that the system has a steady flow.

6) The desired air pressure has been adjusted and injected
7) Once liquid and air conditions are stabilized, the data acquisition system has been started.
8) The flow rate, temperature, pressure, and volume fraction have been monitored and recorded.
9) After recording the necessary outputs, the needle valve and the air pressure regulator have been closed and releases, respectively.
10) The water has been drained

To adjust the inclination the following steps should be followed:

- Ensure that the flow loop system is shut off.
- Release the manual breaks of the frame.
- Set the required degree of inclination
- Lock the manual breaks

3.1.2 Flowzan-Air Experimental Procedure and Data Collection

Extra steps should be added between step (3) and (4) when preparing Flowzan Xan., the steps can be summarized as the following:

1) The amount of the polymer powder has been calculated based on the volumetric concentration required for the test.
2) The agitator has been started at ~ 40-60 rpm.
3) The prepared amount of the polymer has been gradually added using small buckets.
4) Once the polymer powder has been added, the agitation has been continued for about 1-2 hours, or until the required properties are reached.
5) Samples has been taken to check properties like density, viscosity and temperature using the mud balance and thermometer.

3.1.3 Safety Concerns of the Test Setup

a. The flow loop system is equipped with Special designed fasteners that are used to maintain the frame in position and restrict any rotational motion while operating at various inclinations.
b. If for whatever reason the flow encounters extreme conditions exceeding the maximum flowrate and/or pressure that the device can withstand, the system will automatically shut down and stops all operations.
c. There is a PLC system that is attached to the flow regulator to protect it from overheating and further damage.
d. Not to mention, there is a manual emergency button that can used in case the experimenter notices something unusual.

3.1.4 Materials and Operational Conditions

Liquid water was used for the case of the single-phase flow. Newtonian and non-Newtonian fluids were used for the case of two-phase flow. Water (997 kg/m^3) was used as a Newtonian fluid, whereas Flowzan with a concentration of 0.15% was used as the non-Newtonian fluid. The Flowzan (xanthan gum-based high-quality biopolymer) was purchased from Chevron Phillips Chemical Company LP, Texas, United States. Three different inclinations where used, which are 0, 5, and 8 degrees from the horizontal position. The liquid flow rates were varied between 700 to 1100 RPM. The air injection pressure was varied between 1 to 2 bars. The operational conditions of the experiments and the range of properties for water and Flowzan are summarized in Table 3.

Table 3: Operational Conditions for Single and Two-Phase Flow Experiments

Hydrodynamic and Operational Conditions	
Density (water)	997 kg/m^3
Viscosity (water)	0.9 cP
Density (Flowzan)	1005 kg/m^3
Viscosity (Flowzan)	4 cP
Mass flow rate	190 – 350 kg/min
Pump rotational speed	700-1100 RPM
Injection pressure	1-2 bars
Inclination	0 – 8^o

Several test matrices have been planned and developed for single- and two-phase flow experiments under various operational conditions. All are presented in Appendix A, Appendix B, and Appendix C.

3.2 Flow Loop Equipment and Main Components

3.2.1 Frame

The frame of the flow loop system shown in Figure 6, is made of Aluminum. It is worth noting that the frame has been anodized in order to extend its lifetime by converting the metal surface, which is in this case the Aluminum, into a durable and decorative metal with anodic oxide finish. The frame is equipped with some fasteners that provide power locking profile connections of extreme rigidity. A schematic drawing of the frame is shown in Figure 7.

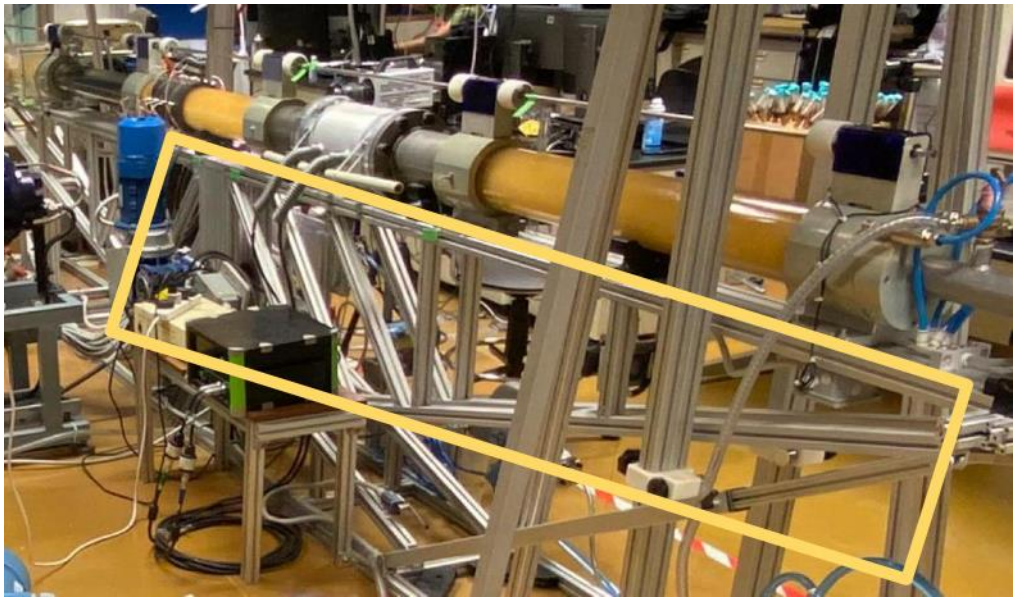

Figure 6: The frame of the flow loop system

The inner diameter of the outer aluminum tube is 4.5 inches. The inner tube is also made of Aluminum. The inner diameter of the inner tube is 2.5 inches. The inner pipe has been fixed by a manual mechanism using locking devices to secure its concentric position as shown in Figure 8.

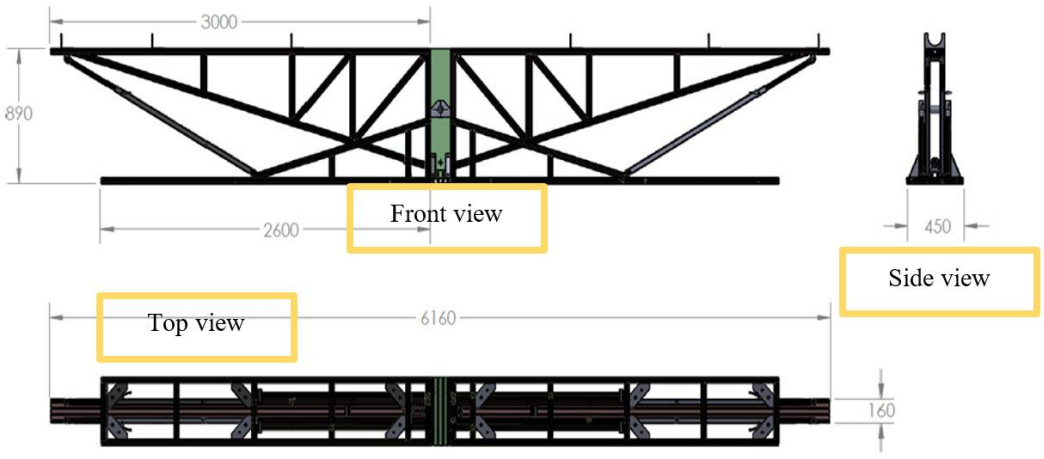

Figure 7: Schematic drawing of the frame

Figure 8: Manual concentricity adjuster

3.2.2 Flange

Several flanges have been applied to the system in order to connect the flow loop piping components together by using gaskets and bolted connections. Figure 9 and Figure 10 are some examples of flanges that have been used in the lab.

The flanges are made of Aluminum 7075 material. Two different Flanges were used:

1) Flanges to connect the components of the main pipe together.
   - The external dimensions of the flanges are Ø 180x150mm.
2) Input and output flanges for two and three phase mixtures (gas, liquid, and solids).
   - The external dimensions of the flanges are Ø 180x200mm.

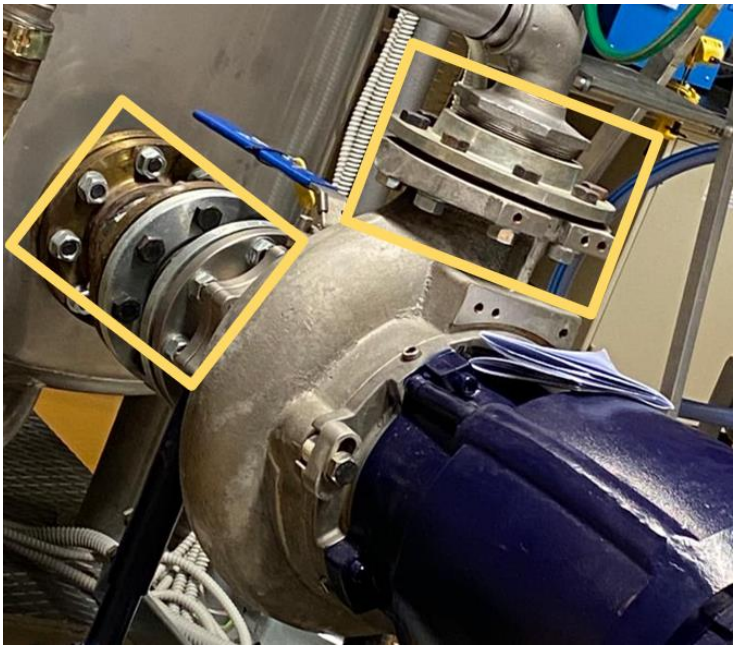

Figure 9: Flanges attached to the tank

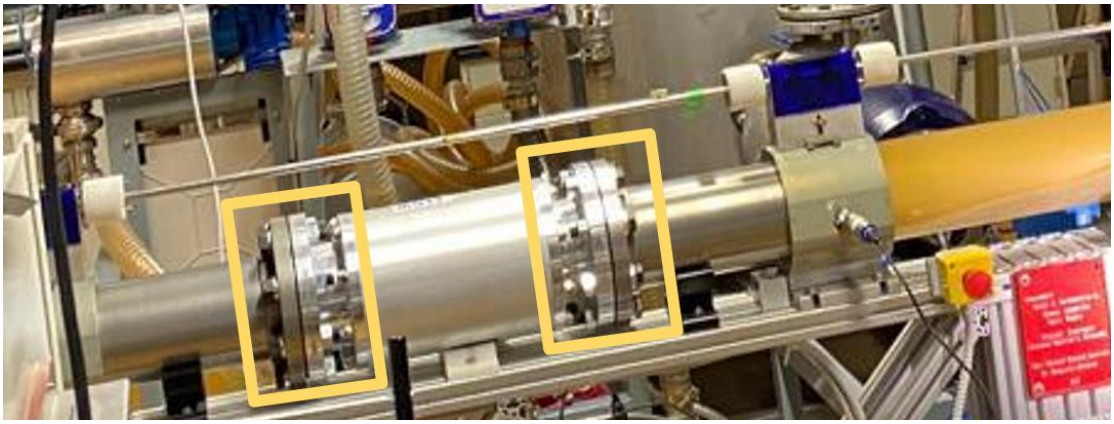

Figure 10: Flanges connect the main pipe together

3.2.3 Pump

As shown in Figure 11, slurry pump has been used in the flow loop multiphase system. The slurry pump can adjust to various flow combinations which varies in solid concentrations, shape and size of solids (if used), in addition to several composition of solutions. The following are some features of the slurry pump:

1) The pump is operating at 12.7 kW which is equivalent to 17 HP.
2) The maximum flow rate of the pump is 21.3 l/s.
3) The rated current can reach up to 20.8 A
4) The maximum frequency that can be achieved is 60 Hz.
5) The maximum pressure that the pump can waistband is 3 barg
6) Can be used for two and three phase flows.
7) Equipped with a 3-phase inverter that converts the direct current (DC) input into an alternating current (AC) output.

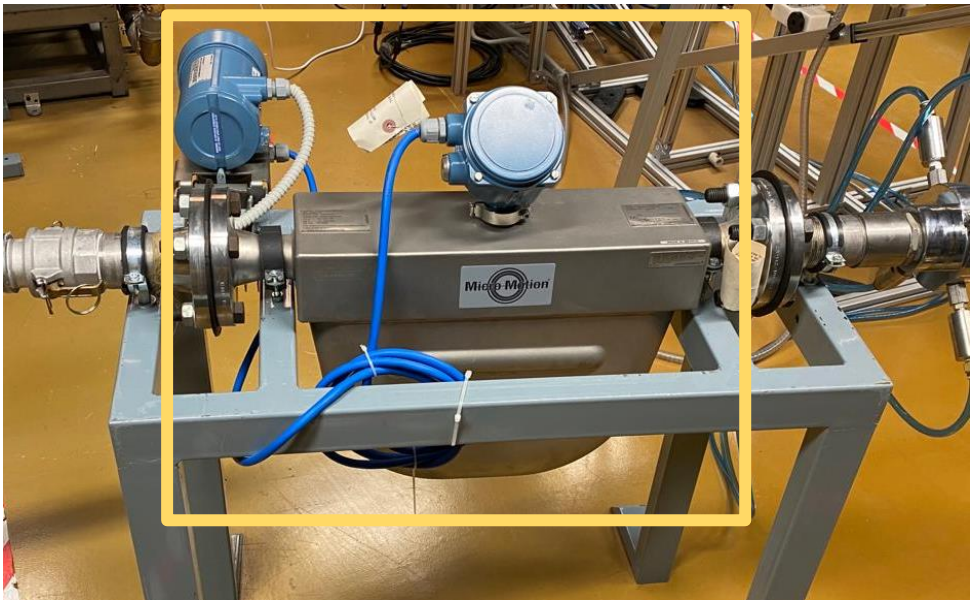

Figure 11: Slurry pump

3.2.4 Flow Meter Sensors

a) Liquid Flow meters

The liquid Coriolis flow meter characterizes with the following:

- Model: F200S Micromotion
- Size and material: 2 inches, 316L stainless steel
- Measures flow rate, density, and temperature of the liquid
- Analog flow reading measure with 4 to 20 mA
- 18 to 100 of Volts Direct Current (VDC) and 85 to 265 Volts Alternating Current (VAC)

b) Gas Flow meter

The gas Coriolis flow meter characterizes with the following:

- Model: F0505S Micromotion
- Size and material: 1/2 inches, 316L stainless steel

- Measures flow rate, density, and temperature of the gas
- Analog flow reading measure with 4 to 20 mA
- 18 to 100 of Volts Direct Current (VDC) and 85 to 265 Volts Alternating Current (VAC)

The device shown in Figure 12, is a digital flow meter that measures the velocity of the injected gas.

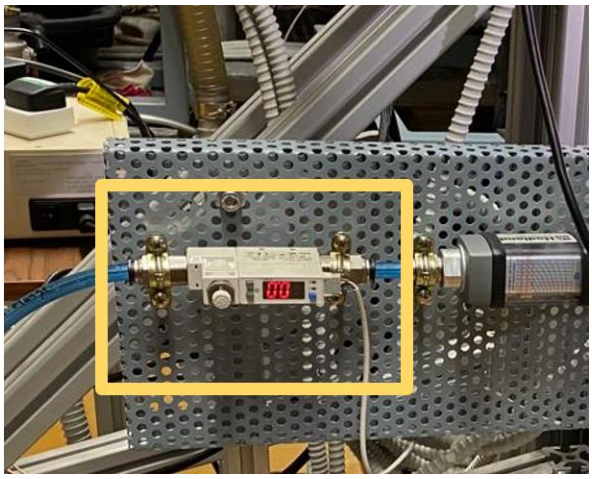

Figure 12: Gas flow meter

c) Digital Multivariate Pressure Transmitter

- Measures absolute and differential pressure
- The transmitter utilizes the highway addressable remote transducer (HART) splitter that communicates between the signals/outputs produced from the instruments and the monitoring devices or central control.
- Operational range is 0-150 psi
- 24 Volts Direct Current (VDC) at 600 ohms

3.2.5 Electrical Cabinet

All of the electrical components are placed inside an electrical cabinet shown in Figure 13. The 120X80X40cm (HxWxD) electrical cabinet is equipped with a residual current device (RCD) and controlling screen, where all of the following parameters can be controlled:

- Setting the RPM of the slurry pump
- Adjusting the inclination angle of the frame
- Controlling the air flow rate of the system
- Controlling the overall system applied pressure
- Controlling the liquid flow rate of the system
- Adjusting the RPM of the agitator

Note that there is a manual emergency button installed in the electrical cabinet to avert arising or to reduce existing hazards (if any).

Figure 13: Electrical cabinet

3.2.6 Programmable Logic Controller

Programmable Logic Controller (PLC) is used to monitor, record, and continuously display the outputs of the sensors, mainly temperature, pressure, and flow rates.

The PLC consists of the following:

- Consists of 10 analog inputs
- 2 analog outputs
- 12 digital inputs
- 8 digital outputs
- 4RS485 ports and one Ethernet.

The PLC is also attached various components like motors, air regulator, level switch, and emergency button.

3.2.7 Electro-Pneumatic Regulator

Regulate and control the inlet of air in the annulus by sending and retrieving signals from the PLC unit.

3.2.8 Motors

The needed power supply for the electrical components is as the following:

- 14 kW for 3-phase inverter in the slurry pump.
- 2.2 kW (1HP) for inclining / declining the angle.
- 0.7 kW for the revolutions of the agitator.
- 1 KW for tube rotation with the RPM ranging between 10 to 200.

3.2.9 Hydro cyclone

The hydrocyclone shown in Figure 14, is a gravity separator device, that uses the pressure of the fluid to generate centrifugal force in order to separate the slurry product mainly phases based on particles weight from the bulk fluid. The device separates particles that have similar sizes but distinct specific gravities, or similar specific gravities by distinct particle sizes.

The specifications of the hydrocyclone are as follows:

1) It consists of two inlets and two outlets.
2) Made of INOX material, which is a steel-based material that considered to be a good resistance against corrosion and acids.
3) The operating pressure is ranging from 2 to 4 bars.

Figure 14: Hydrocyclone device

3.2.10 Tank

There are two tanks available in the lab as illustrated Figure 15 and Figure 16. The characterizations of the tanks are as the following:

- The total capacity of the main tank is around1000 Liters.
- The total capacity of the mixing tank is around 300 Liters
- The tanks have a thickness of 2 mm
- The main tank is connected to the flow loop and to a drain pump
- The small mixing tank is equipped with an agitator that ensures an appropriate mixing of solid and liquid, or to prepare a non-Newtonian fluid by mixing some additives like a bio-based polymer with liquid water.

Figure 15: Main tank

Figure 16: Small mixing tank

3.2.11 Gas Injection Device

Introducing the air into the system in multiphase experiments is essential. As shown in Figure 17, the air injection system can be controlled using three components, which are as follows:

Component A: This component is called the pressure gauge. This instrument measures and displays the applied air pressure.

Component B: This component controls the air pressure that will be introduced into the system. In this study, the air injection pressure was increased up to a maximum value of 2 bars and decreased down to a minimum value of 1 bar.

Component C: This is a manual switch that is being used to inject the specified pressure into the system for the any period of time.

The air pressure was injected into the system by using the air tubes shown in Figure 18, that are attached to the main flow loop pipe.

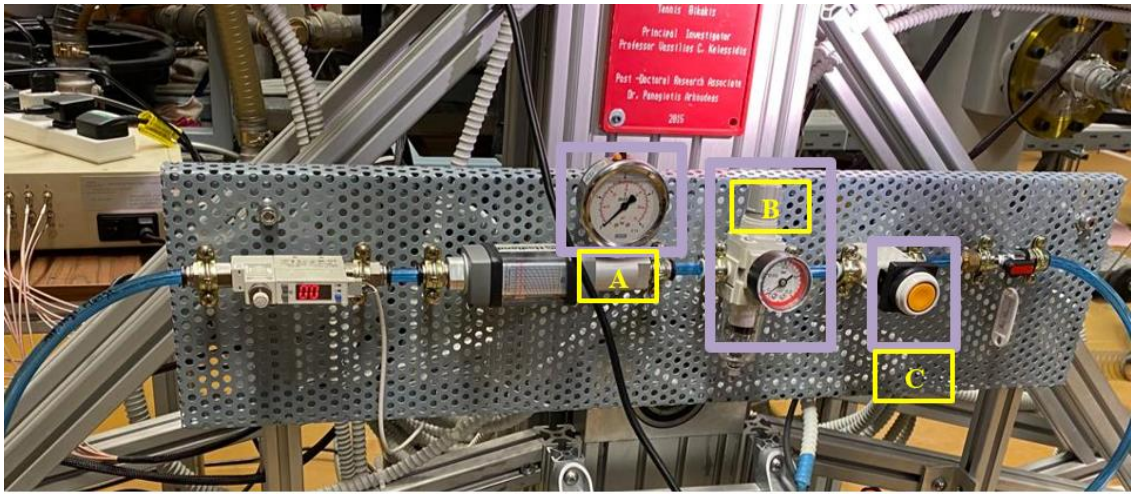

Figure 17: Air injection system

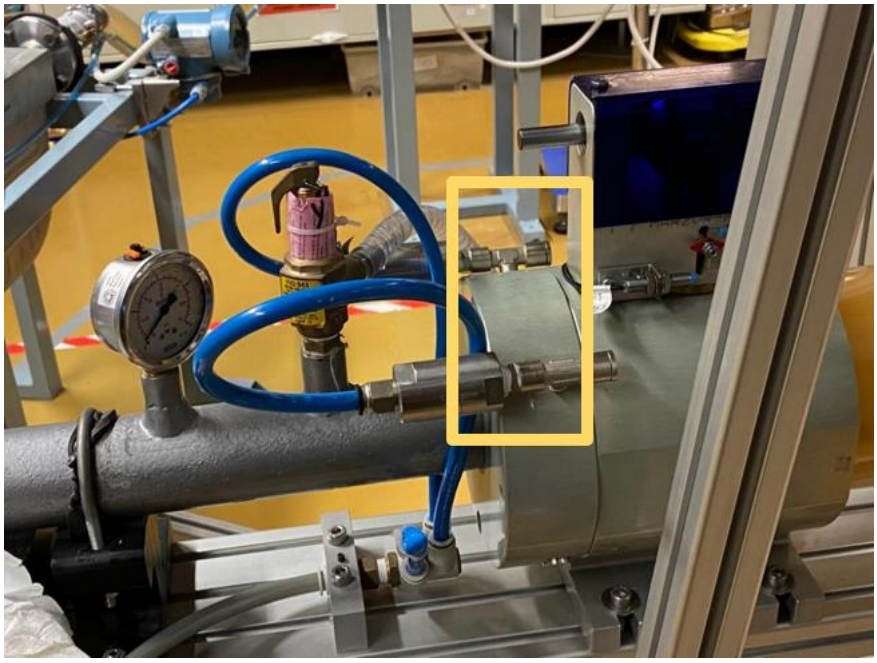

Figure 18: Injection tubes

3.2.12 Pressure sensors

Two dynamic pressure sensors have been used to record the change of pressure along the annular pipe at two different locations. The dynamic sensor that has been used in single- and two-phase flow experiments is shown in Figure 19. The specifications of the dynamic pressure sensor are presented in Table 4.

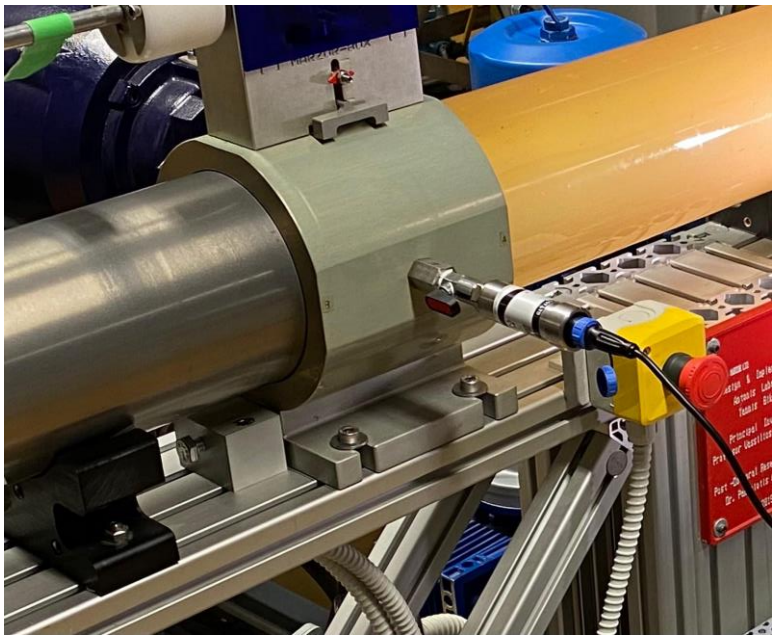

Figure 19: Dynamic pressure sensor

Table 4: Specifications of the dynamic pressure sensor

Specifications	
Model	GD4200-USB
Sampling rate	Up to 1,000 Hz
Accuracy	±0.15%
Pressure range	-1 to 2.5 barg
Resolution	Extremely high 21-bit resolution

3.3 Theoretical Models

3.3.1 Basic Parameters in Multiphase Flow

The time-averaged void/liquid hold up fraction of the ith phase in a section of the pipe is the general definition of the mean phase content, sometimes it is described as the time-averaged area fraction of the ith phase. The mean phase content is referred by ε_i which describes the amount of gas and liquid presented in the flow. The U_i is considered to be the superficial flow velocity or volume flux of a certain phase and it is hypothetical flow velocity, which calculated based on an assumption that each phase is the only one flowing inside the pipe, and it is defined as the following:

$$U_i = \frac{\dot{V}_i}{S} \tag{15}$$

The volume flow rate represented in $\dot{V}_i$ with m^3/s which provides a measurement of the bulk amount of liquid or gas phases, whereas the channel's cross-sectional area represented in S with m^2. The overall volume flux or superficial flow velocity can be calculated as the following:

$$U = \sum_{i-1}^{n} U_i \tag{16}$$

The symbol n represents the number of all phases flowing inside the pipe, it is 2 in case of two-phase flow, and 3 in case of three phase flow. Below is the equation for the average phase velocity u_i:

$$u_i = \frac{U_i}{\varepsilon_i} = \frac{U_i}{S\varepsilon_i} \tag{17}$$

The following is the flow quality of the ith phase represented in x_i:

$$x_i = \frac{\dot{m}_\iota}{\sum_{i-1}^{n} \dot{m}_\iota} \tag{18}$$

The mass flux of the phases is represented as $\dot{m}_\iota$, which can be calculated by dividing the mass flow rate of the flow of the ith phase $\dot{M}_\iota$ over the total cross-sectional area of the pipe. For multiphase flow, the mixture density ρ_{MP} can be calculated using the following equation:

$$\rho_{MP} = \sum_{i-1}^{n} \varepsilon_i \rho_i \tag{19}$$

3.3.2 Homogenous Model

The homogenous model is considered to be the simplest one among multiphase models, because this approach treats the properties and velocities as a mixture of the two phases. The following is the homogenous velocity represented by u_H:

$$u_H = U = \frac{\dot{m}_\iota}{\rho_H} = \frac{\dot{M}}{S * \rho_H} \tag{20}$$

$$\rho_H = \frac{\dot{m}}{U} = \frac{1}{\sum_{i-1}^{n} \frac{x_i}{\rho_i}} \tag{21}$$

Where:

$\dot{m}$: is the total mass flux,

$\dot{M}$: the total mass rate of flow.

ρ_H: is *the homogeneous density.*

The conservation of energy, momentum and mass for the homogenous approach are represented by [74]:

$$\frac{\partial}{\partial z}(U\,\rho_H S) + S\frac{\partial \rho_H}{\partial t} = 0 \tag{22}$$

$$\frac{\partial \dot{m}}{\partial t} + \frac{1}{S}\frac{\partial(\frac{\dot{m}^2 S}{\rho_H})}{\partial z} = \frac{\partial \rho}{\partial z} - g\rho_H \sin(\alpha) - \frac{\tau_o P}{S} \tag{23}$$

$$\rho_H\left(\frac{\partial e}{\partial t} + U\frac{\partial e}{\partial z}\right) = \frac{\dot{q}P}{S} + \dot{q}_v + \frac{\partial p}{\partial t}$$

Where, τ_o is the shear stress at the wall, $\dot{q}$ is the heat flux at the wall, and $\dot{q}_v$ is the internal heat generation.

The energy converted per unit fluid mass represented in e can be calculated using the following equation:

$$e = h + \frac{u^2}{2} + g * z * sinc(\alpha) \tag{24}$$

z the axial distance, and h is the specific enthalpy which can be calculated using the following equation:

$$h = \mu_{specific} + \frac{p}{\rho_H} \tag{25}$$

Where, μ_{specific} is the specific internal energy.

The conservation of momentum can be simplified to the following equation if the steady state is assumed as a constant along the pipe:

$$-\frac{dp}{dz} = \frac{\tau_o P}{S} + \frac{\dot{m}^2 \left(\frac{1}{\rho_H}\right)}{dz} + g\rho_H \sin(\alpha) \tag{26}$$

3.3.3 Separated Flow Model

As shown in Figure 20, in the separated flow model, the phases are assumed to flow independently in separated zones of the pipe. Each phase will have its own properties and velocities.

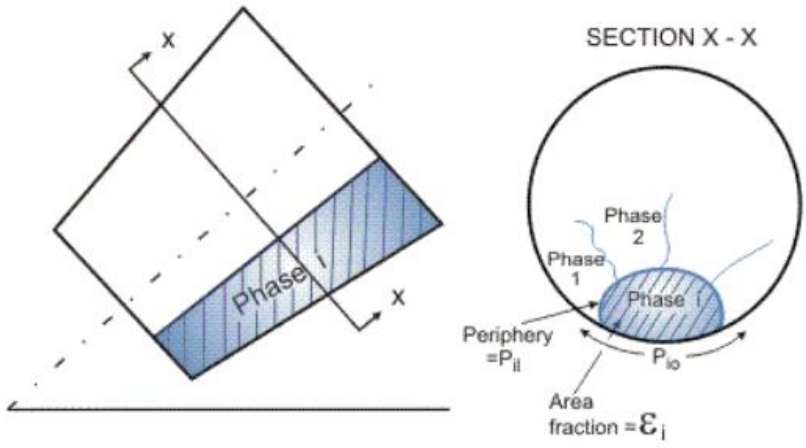

Figure 20: Separated phases [74]

In order to develop equations for the separated model approach, the conservation of energy, momentum and mass can be written for each phase separately by taking into consideration the interaction between the phases and pipe wall. The following are the multiphase energy, momentum, and mass conservation equations for the separated model approach:

$$\frac{\partial}{\partial t}(\rho_{MP}S) + \frac{\partial}{\partial z}(\dot{m}S) = 0 \tag{27}$$

$$-\frac{\partial p}{\partial z} - g\rho_{MP}\sin(\alpha) - \frac{\sum_{i-1}^{n}\tau_o\rho_0}{S} = \frac{\partial \dot{m}}{\partial t} + \frac{1}{s}\frac{\partial}{\partial z}(\dot{m}^2 S\sum_{i-1}^{n}\frac{x_i^2}{\varepsilon_i\rho_i}) \tag{28}$$

$$S\frac{\partial}{\partial t}\left(\sum_{i-1}^{n}\varepsilon_i\rho_i h_i\right) + \frac{\partial}{\partial z}\left(S\sum_{i-1}^{n}\dot{m}x_i h_i\right) = \dot{q}p + \dot{q}_m S - \frac{\partial}{\partial z}\left(\dot{m}^2 S\sum_{i-1}^{n}\frac{x_i^3}{(\varepsilon_i\rho_i)^2}\right) - g * \dot{m} * S * sin(\alpha) - \frac{\partial}{\partial t}\left(\dot{m}^2\sum_{i-1}^{n}\frac{x_i^2}{\varepsilon_i\rho_i}\right) + S\frac{\partial p}{\partial t} \tag{29}$$

Where, ρ_i is the density of the ith phase and h_i is the enthalpy of the ith phase.

As the homogenous model, the conservation of momentum can be simplified to the following equation if the flow is steady state:

$$-\frac{dp}{dz} = \frac{\tau_o P}{S} + \dot{m}^2\frac{d}{dz}(\sum_{i-1}^{n}\frac{x_i^2}{\varepsilon_i\rho_i}) + g\rho_H\sin(\alpha) \tag{30}$$

3.3.4 Beggs and Brill Correlation

First, boundaries of the correlation should be defined as the following:

$$L_1 = (316)C_L^{0.302} \tag{31}$$

$$L_2 = (9.252 * 10^{-4}).C_L^{-2.4684} \tag{32}$$

$$L_3 = (0.1)C_L^{-1.4516} \tag{33}$$

$$L_4 = (0.5)C_L^{-6.738} \tag{34}$$

By using the correlation boundaries described above, the flow pattern will be determined according to the following conditions:

For the intermittent flow:

$$L_3 < Fr_H \leq L_1 \ \& \ 0.01 \leq C_L < 0.4 \quad (35)$$

$$L_3 < Fr_H \leq L_4 \ \& \ C_L \geq 0.4 \quad (36)$$

For the segregated flow:

$$Fr_H < L_1 \ \& \ C_L < 0.01 \quad (37)$$

$$Fr_H < L_2 \ \& \ C_L \geq 0.01 \quad (38)$$

For the transition flow:

$$L_2 \leq Fr_H \leq L_3 \ \& \ C_L \geq 0.01 \quad (39)$$

For the distributed flow:

$$Fr_H \geq L_1 \ \& \ C_L < 0.4 \quad (40)$$

$$Fr_H > L_4 \ \& \ C_L \geq 0.4 \quad (41)$$

Where the Froude number can be calculated as the following:

$$Fr_H = \frac{u_H^2}{g.d_h} \quad (42)$$

It is worth mentioning that conditions for each of the aforementioned patterns are considered to be a grouping to some other flow patterns as the following:

1) The intermittent flow: includes plug and slug flow.
2) The segregated flow: includes the annular, stratified and wavy flow.
3) The transition flow: represents the transitions from segregated flow patterns into intermittent flow patterns.
4) The distributed flow: includes the bubbly flow.

There is a separate calculation of liquid holdup $E_L(0)$ for each flow type by using the following equations:

For the distributed flow:

$$E_L(0) = \frac{1.065 C_L^{0.5824}}{Fr_H^{0.0609}} \tag{43}$$

For the segregated flow:

$$E_L(0) = \frac{0.98 C_L^{0.4846}}{Fr_H^{0.0868}} \tag{44}$$

For the transition flow:

$$E_L(0) = \left(\frac{L_3 - Fr_H}{L_3 - L_2}\right) * \left(\frac{0.98.\, C_L^{0.4846}}{Fr_H^{0.0868}}\right) + \left(1 - \frac{L_3 - Fr_H}{L_3 - L_2}\right) * \left(\frac{0.845 C_L^{0.5351}}{Fr_H^{0.0173}}\right) \tag{45}$$

For the intermittent flow:

$$E_L(0) = \frac{0.845 C_L^{0.5351}}{Fr_H^{0.0173}} \tag{46}$$

The two-phase friction factor is defined as the following:

$$\frac{f_{tp}}{f_{NS}} = e^S \tag{47}$$

Therefore,

$$f_{tp} = f_{NS} * e^S \tag{48}$$

Where, f_{NS} is the no-slip friction factor based on the no-slip Reynolds number. The constant S is required to determine the two-phase friction factor f_{tp}.

The exponent S, is empirically related to the parameter y, and can be calculated as the following:

If $1 < y < 1.2$, then:

$$S = \ln(2.2y - 1.2) \tag{49}$$

Otherwise, when $y > 1.2$:

$$S = \frac{\ln(y)}{-0.0523 + 3.182\ln(y) - 0.8725(\ln(y))^2 + 0.01853)(\ln(y))^4} \tag{50}$$

Where,

$$y = \frac{C_L}{E_L^2} \tag{51}$$

For inclined systems, the actual volume fraction can be obtained by using the following inclination factor:

$$E_L(\theta) = B(\theta) x E_L(0) \tag{52}$$

Where,

$$B(\theta) = 1 + Z[Sin(1.8\theta) - \frac{1}{3}\sin^3(1.8\theta)] \tag{53}$$

From Equation (55), Z can be calculated as the following:

For Uphill flow:

Segregated

$$Z = (1 - C_L)\ln\left[\frac{0.011 N_{lv}^{3.539}}{C_L^{3.768} Fr_H^{1.614}}\right] \tag{54}$$

Intermittent

$$Z = (1 - C_L)\ln\left[\frac{2.96 C_L^{0.305} Fr_H^{0.0978}}{N_{lv}^{0.4473}}\right] \tag{55}$$

Distributed

$$Z = 0 \tag{56}$$

For Downhill flow:

$$Z = (1 - C_L)\ln\left[\frac{4.70\ N_{lv}^{0.1244}}{C_L^{0.3692} Fr_H^{0.5056}}\right] \quad (57)$$

The total pressure gradient is represented as the following:

$$-\frac{dp}{dz} = \frac{g}{g_c}\rho_{tf}\sin(\theta) + \frac{f_{tp} G_m v_m}{2 g_c d} - \frac{\rho_{tf} v_m v_{sg}}{g_c p}\frac{dp}{dz} \quad (58)$$

It can also be represented as:

$$-\frac{dp}{dz} = \frac{\frac{g}{g_c}\rho_{tf}\sin(\theta) + \frac{f_{tp} G_m v_m}{2 g_c d}}{1 - \rho_{tf} v_m v_{sg}/g_c p} \quad (59)$$

Where,

$$\rho_{tf} = \rho_L H_L + \rho_g (1 - H_L) \quad (60)$$

3.4 Development of the Computation Fluid Dynamic Model

A numerical simulation was performed on an annular horizontal and near horizontal pipe. Two-phase Gas-liquid system was used with constant properties of density and viscosity. The CFD model was developed as per the following steps:

3.4.1 Geometry

The first step is constructing the geometry. A 2D sketch of annular cross section was made using the same dimensions as the experimental set-up with outer and inner diameters of 6.35 cm (2.5 inch), and 11.43 cm (4.5 in). The sketch was then extruded. Two new planes have been drawn, the planes were used to locate and extrude the air injection tubes. There are two air injectors, each with 0.012 m diameter. The injectors have been sliced, to efficiently control the mesh of each region. The geometry model is shown in Figure 21.

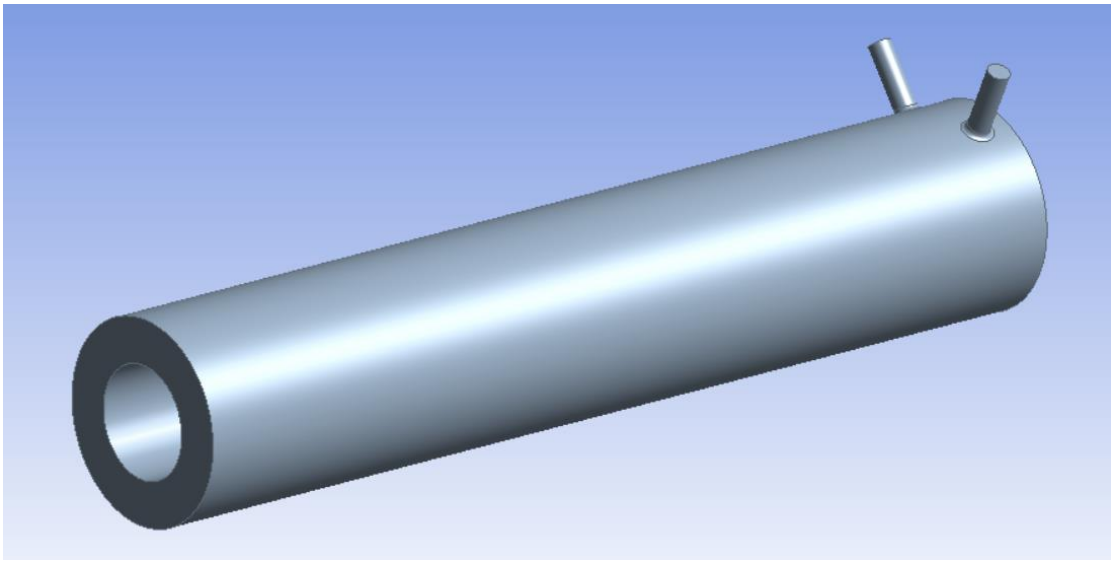

Figure 21: CAD geometry

3.4.2 Meshing

The second step is defining the mesh as shown in Figure 22 and Figure 23. Tetrahedral elements mesh method was used. The total number of elements is 260,378 whereas the total number of nodes is 254,579. Then face messaging was applied on the inlets and outlet with 40 number of divisions to ensure accurate results.

After that, the main parts of the pipe have been named using create named selection option, which are as the following:

1) liquid inlet.
2) Inlets for the gas.
3) Outlet (Mixture of gas and liquid).
4) Outer and inner walls.

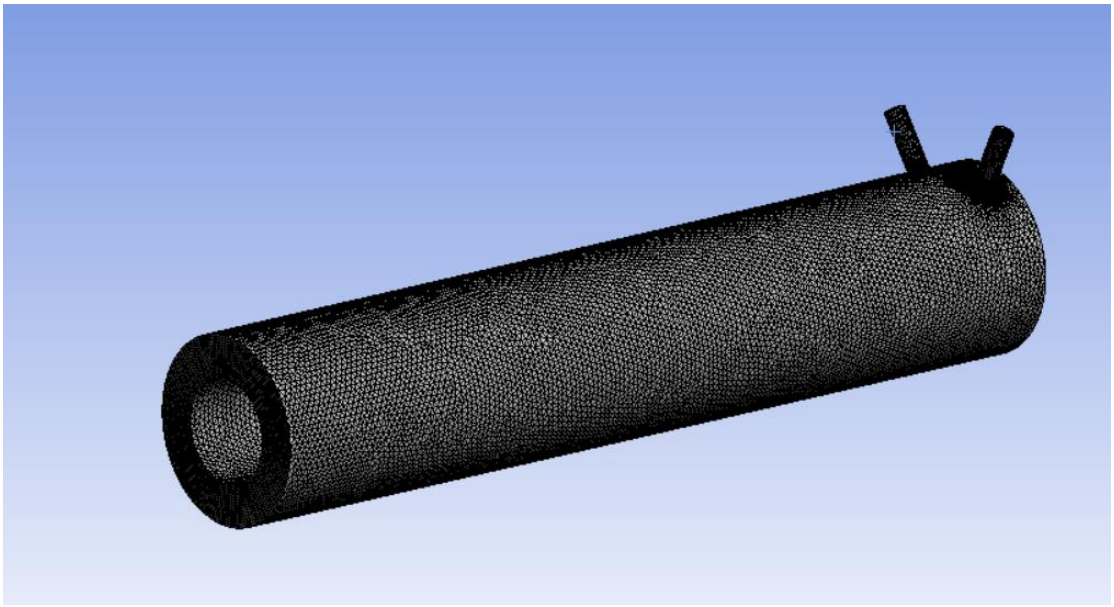

Figure 22: CAD meshing, isometric view

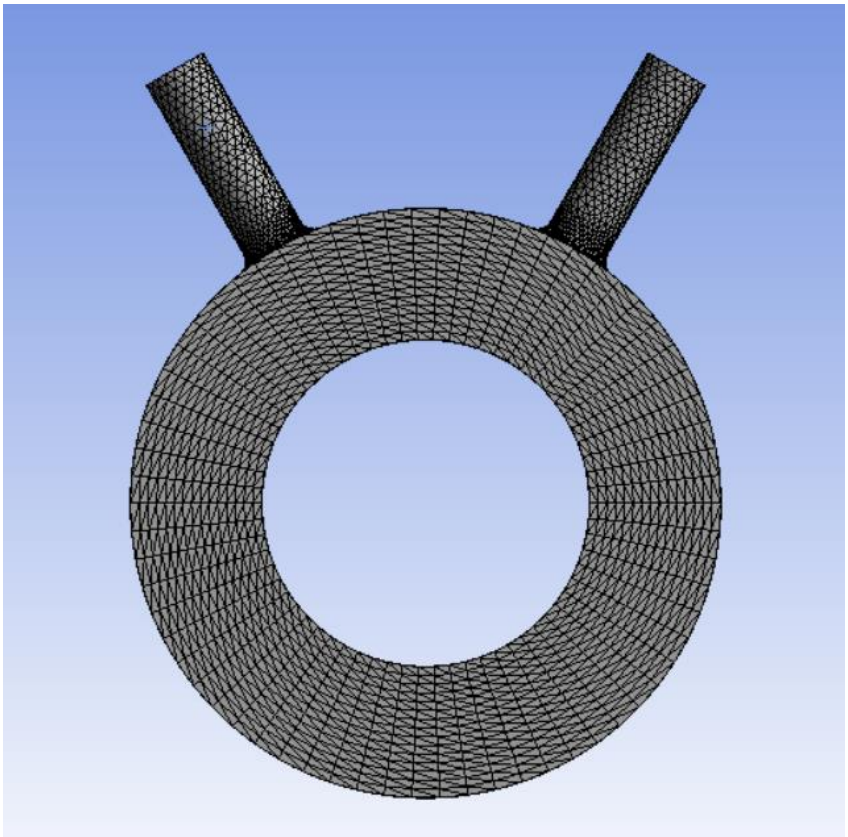

Figure 23: CAD meshing, side view

3.4.3 Setting Up the Model

Setting up the model in ANSYS workbench is considered to be an essential step prior to simulation. In this work, to accurately predict the pressure drop in two-phase liquid-air flow through annular cross-sectional tube, the following was implemented:

- The Multiphase model has been chosen as Eulerian-Eulerian as this approach ensures maximum accuracy for liquid-air phase flow.
- Shear stress transport (SST) model has been used as the Turbulence model.
- The initial conditions have been defined as per the experimental conditions.
- SIMPLE algorithm is used for the pressure velocity coupling.
- The QUICK method was used in the spatial discretization.
- The second order upwind scheme was used for the rest of the equations.
- The interface model has been taken into consideration, including drag, lift and wall lubrication forces.
- The Grace model was used for dragging force.
- The Tomiyama model for lifting force.
- The Hosokawa model for wall lubrication force.

CHAPTER 4: RESULTS AND DISCUSSION

This chapter presents multiple experimental results for single- and two-phase flows. The section started by describing the calibration of the dynamic pressure sensors. After that, the repeatability test was performed in order to ensure that the obtained results are repeatable and reproducible. The results for single- and two-phase flow have been compared with the theoretical correlations. Finally, a two-phase CFD model has been developed and then the accuracy of the predictions has been judged by making a comparison with the actual results and theoretical models.

4.1 Calibration of the Dynamic Pressure Sensors

Two pressure sensors were used to measure the pressure of the air-water mixture at two different locations along the test section. The pressure sensors were positioned 3.3 meters apart. The dynamic pressure sensors were automatically calibrated using the control software that is attached to the data acquisition system. The respective calibration outputs of the dynamic pressure sensors were matching with the input pressure in the flow loop system which is 1 bar as shown in Figure 24.

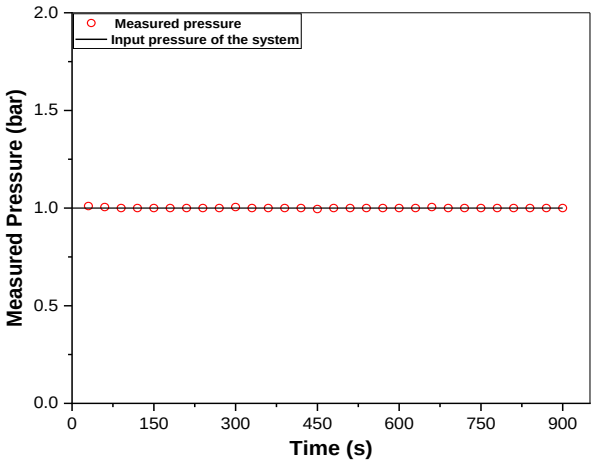

Figure 24: Calibration of dynamic pressure sensors

4.2 Single Phase Flow

4.2.1 Repeatability Test

To ensure having robust and reliable data, the repeatability test (which sometimes called test–retest reliability) was performed, this test evaluates how repeatable the results are under a set of similar conditions. This test also considered as an efficient way of measuring precision, and it is being used on this test rig in order to assess the findings and confirm the accuracy of the data and the outcomes that will be generated and concluded, respectively. The closeness of agreement between the results of successive measurements was as high as ≅ 98.64%. Figure 25 illustrates the robustness of the system by comparing two experimental runs operating under the same conditions. The conditions of the two runs are presented in Table 5.

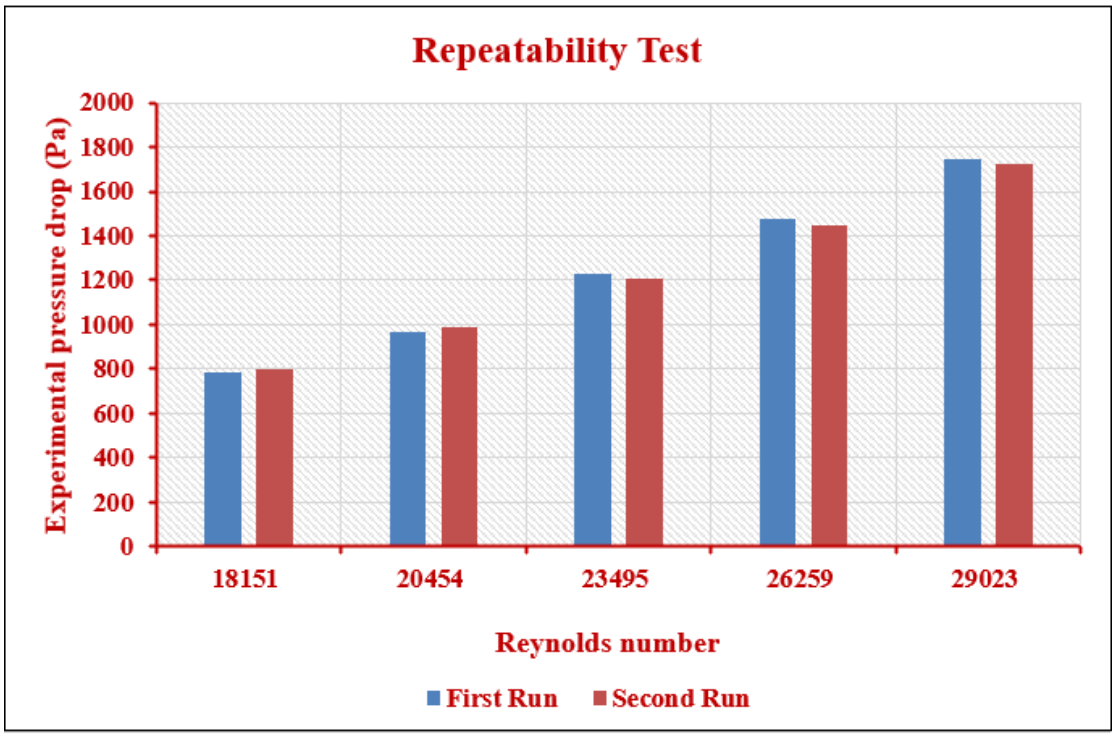

Figure 25: Repeatability test of the experimental pressure drop for two experiments

The pressure drop of the two runs was measured using the dynamic pressure sensors. Looking at the results, the average variation of the pressure difference is 1.36%, with a maximum and minimum variations of 1.74% and 0.98%, respectively. Hence, the data produced from the flow loop system is considered to be repeatable and reproducible.

Table 5: Operational Conditions for the Repeatability Test

Operational Conditions	
Phase of flow	Single phase
Working fluid	Liquid (Water)
Flow rate (kg/min)	192-315
Inclination (^{o}) From horizontal position	0
Number of experiments	10
Number of runs (for each experiment)	2

4.2.2 Experimental Pressure Drop Measurements

In single phase flow, the experiments were conducted with varying the inlet liquid flow rates in addition to the inclination angles. The liquid flow rates were varied between 192-315 kg/min. For each flow rate, three different inclinations were used, including the horizontal case (0 degrees), 5 degrees, and 8 degrees. A summary of the operational conditions and flow properties are presented in Table 6.

Table 6: Operational Conditions

Operational Conditions	
Phase of flow	Single phase
Working fluid	Liquid (Water)
Density (kg/m^3)	997
Viscosity (Pa.s)	0.009
Pump rotational speed (RPM)	700-1100
Flow rate (Kg/min)	192-315
Inclination (^{o}) From horizontal position	0, 5 & 8
Pressure (bar)	1

Figure 26 summarizes the results of the experimental work performed for the conditions described above. It can be noticed that the pressure drop increases with increasing the liquid flow rate, this behavior applies for all the inclinations. Furthermore, at a constant flow rate, the pressure drop increases significantly with increasing the inclination angle from 0 to 8 degrees. A validation of the described behavior is needed, which is done in the next part.

4.2.3 Theoretical Model

A mathematical theoretical correlation was used to validate the experimental pressure drop values. It can be noticed from Figure 26 that in comparison with the horizontal case, the error in the pressure drop was noticeable for higher inclination angles (5 and 8), and that in fact has something to do with the absolute error. The average absolute error variations were found as follows: 41 Pa at 0, 141 Pa for 5, and 138 Pa for 8

degrees. However, the calculated average relative error between the experimental and theoretical pressure drop is 3.9% at 0 degrees, 3.2% at 5 degrees and 2.89% at 8 degrees. According to Figure 26, and based on the average absolute and relative errors, it can be concluded that there is a good agreement between the experimental results and the theoretical model for the single-phase flow.

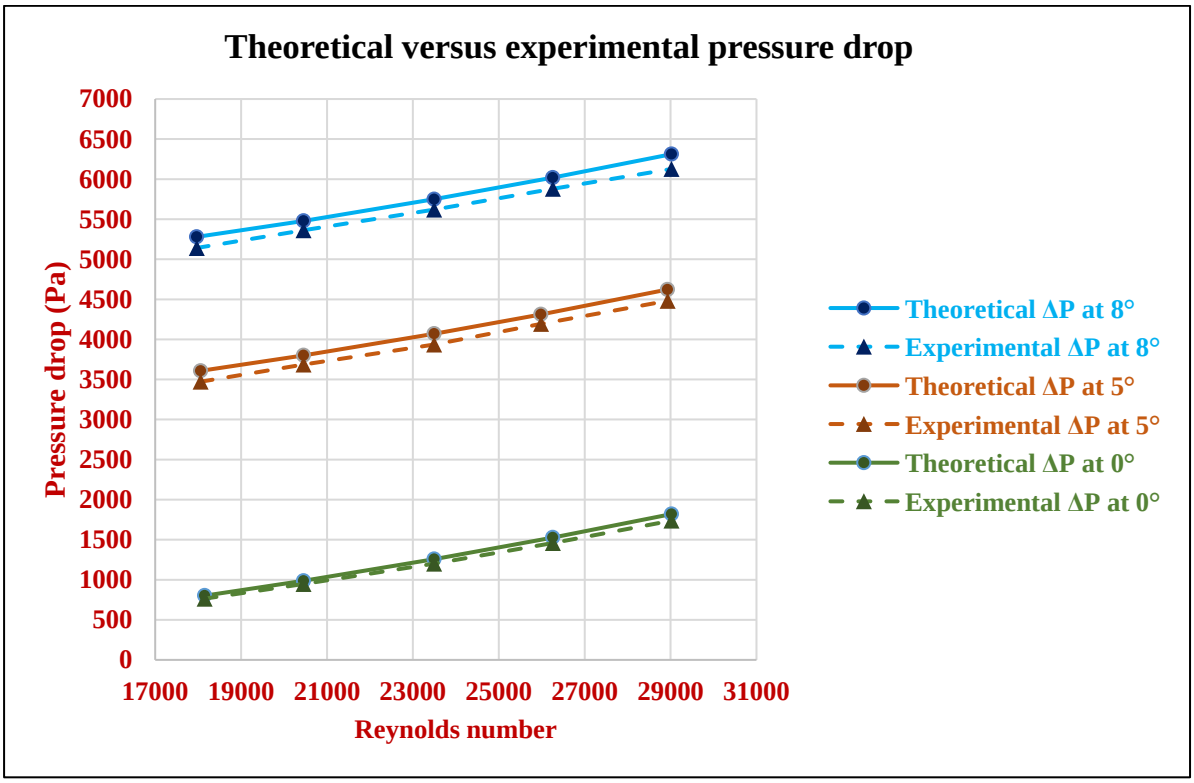

Figure 26: Validation of the experimental results

4.3 Two-Phase Flow (Water-Air)

In two-phase flow experiments, two different combinations of liquid-air phases were taken into consideration, the first combination is Water-Air which treated the water as a Newtonian fluid, and the second one utilized a bio-based polymer represented in xanthan gum, that produced a combination of Flowzan-Air, in which Flowzan is treated as a non-Newtonian fluid.

Finding and evaluating the frictional pressure drop in two-phase flow in both of the experimental and theoretical approaches is considered to be much more complicated than that in single-phase flow, as the two-phase pressure drop is associated with the interaction of phases along with the momentum exchange between the liquid and gas flow phases.

In the following section, a study will be performed to accurately describe the behavior of the experimental pressure drop in two-phase flow. Then, various theoretical correlations will be judged based on a comparison between the actual and the predicted pressure drop results.

4.3.1 Water-Air Experiments

Multiple experiments were conducted using the Water-Air phase flow. The flow rates were varied in the rage of 192-315 kg/min. Different inclination angles were used between 0-8 degrees. The applied pressure was varied between 1-2 bars. A summary of the operational conditions is presented in Table 7.

Table 7: Two-Phase Operational Conditions

Operational Conditions	
Phase of flow	Two-phase
Working fluid	Liquid-Gas (Water-Air)
Pump rotational speed (RPM)	700-1100
Flow rate (Kg/min)	192-315
Inclination (from horizontal)	0, 5 & 8
Air injection Pressure	1-2 bars

Figure 27 represent the experimental pressure drop results for 0,5 and 8 degrees of upward inclination. Generally, it can be noticed that both of the liquid flow rate and air injection pressure are positively correlated with the pressure drop, as increasing either of them separately while keeping the other one constant will result in an increase in the pressure drop.

Additionally, it can be observed that the impact of increasing the mass flow rate on the pressure drop is much higher than the impact of increasing the gas injection pressure by considering the operating conditions that have been applied to the system.
Taking the first point in the case of 8 degrees as an example, the pressure drop increases by around 49 pa by increasing the injection pressure from 1 to 2 bars, however, at a constant air pressure, and by increasing the pump rotational speed from 700 to 800 RPM, or from 192 to 222 kg/min, an increase of 98 pa in pressure drop was noticed, which is almost the double when compared to the effect of changing the injection pressure.

Also, it can be noticed that the pressure of the two-phase flow increases as the air injection pressure is increasing from 1 to 2 bars, and that is due to the friction increase. At constant liquid mass flow rate, increasing the gas injection pressure will increase the velocity of the injected gas, and that would result in a higher pressure drop value. This is consistent with two-phase flow correlations available in literature as shown in section 3.3, for example Equation (58).

The effect of increasing the inclination can also be seen from Figure 27. Taking the flow rate of 192 kg/min as an example, the pressure increases from 400 Pa to 1100 Pa

by increasing the angle from 0 to 5 degrees, and from 1100 Pa to 1600 Pa by increasing the angle from 5 to 8 degrees.

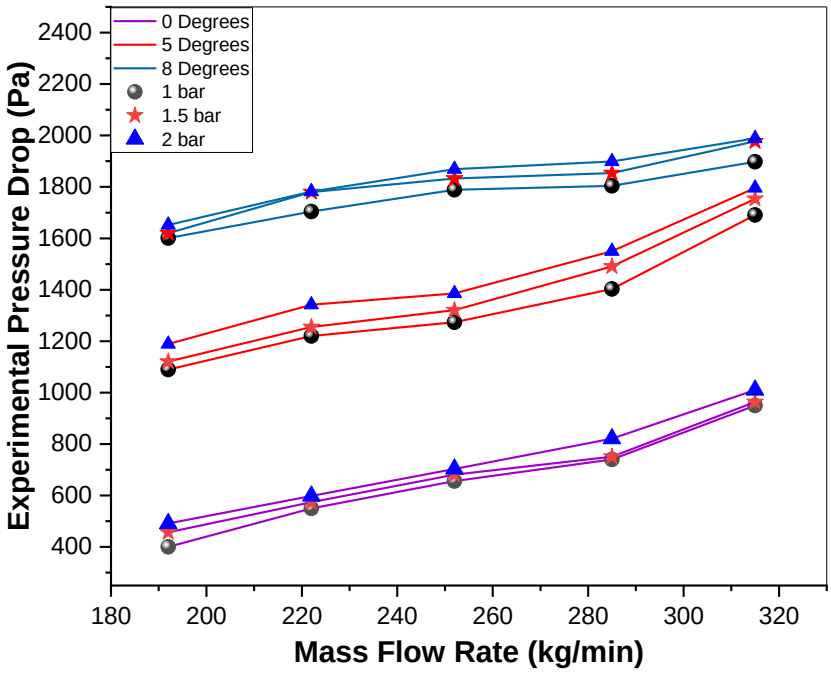

Figure 27: Experimental pressure drop at 0, 5, and 8 degrees of inclination for a range of water flow rate and inlet air pressure.

4.3.2 Theoretical Correlations

Several theoretical approaches that were developed based on a circular cross-sectional geometry will be used in this study by comparing them with the experimental results using the concept of hydraulic diameter. These correlations are currently being used to predict the pressure drop of two-phase gas-liquid flow for both circular and annular geometries. The theoretical models are Dukler's and Shannak's homogeneous models, Lockhart-Martinelli's separated model, in addition to Beggs & Brill model.

Figure 28 presents a comparison between the experimental pressure drop data with Dukler's and Shannak's homogenous theoretical models at 0, 5, and 8 degrees at gas injection pressure of 1, 1.5 and 2 bars.

In Figure 28a, both of the measured and homogenous data have an increasing trend with respect to the liquid mass flow rate. The same behavior can be observed for the conditions in Figure 28b and Figure 28c. In terms of the pressure drop, it can be noticed that there is a variation between the measured data and both of Dukler's and Shannak's homogenous models, as the average pressure drop variations are 371.3 Pa, 395.6 Pa, and 432.6 Pa for 1, 1.5 and 2 bars.

Taking the first point as an example, for the injection pressure of 1,1.5, and 2 bars and at a constant liquid flow rate of 192 $\mathrm{kg/min}$, the measured pressure drops were 400 Pa, 457 Pa and 491 Pa, while Dukler's homogenous pressure drops are 172.7 Pa, 176 Pa, and 178.4 Pa. Meaning, the homogenous model underestimates the measured pressure drop as the impact of increasing the injection pressure is much lower in the case of homogeneous model than the actual measured data.

At an inclination angle of 5 degrees, the Dukler's and Shannak's homogenous models severely overestimated the pressure drop for all cases of 1, 1.5, and 2 bars from Figure 28d to Figure 28f, and the variation is huge compared to the case of 0 degrees. At flow rate of 192 $\mathrm{kg/m^3}$, the absolute average variations are 1731.4 Pa, 1680.3 Pa, and 1618.2 Pa for the injection pressure of 1,1.5, and 2 bars. The increase of the variations compared the 0 degrees case indicates that using Dukler's and Shannak's homogeneous models cannot accurately account for the increase of inclination angles.

In comparison with 0 and 5 degrees, and as shown from Figure 28g to Figure 28I, the 8 degrees of inclination results in the highest pressure drop variations by overestimating the experimental pressure drop. For the injection pressure of 1,1.5, and 2 bars, the variations between the measured data and both of Dukler's and Shannak's homogenous pressure drop models are 2970.9 Pa, 2918.6 Pa, and 2894.6 Pa. Thus, a comparative relation can be concluded, as the more the inclination angles increase, the less the homogenous models can account for the inclination angles.

Not only the homogeneous models do not accurately predict the actual pressure drop values but also they do not simulate the actual behavior of pressure drop with respect to the liquid mass flow rate, as the homogenous models in all of the previous conditions are acting more like a linear function.

The homogenous models failed to calculate the pressure drop through annular cross-sectional pipe. The implementation of the hydraulic diameter concept is the major factor that has contributed to that huge variation, as this correlation was developed based on a circular cross-sectional pipe. However, and generally speaking, there are other weaknesses associated with the homogeneous model it-self, as assuming that the two-phases of gas-liquid are travelling at the same velocity (which is the central assumption of the homogeneous approach) is not appreciated in the case of two-phase flow because in most real-life applications specially in the oil and gas industry, the phases do not have the same velocity.

(a)

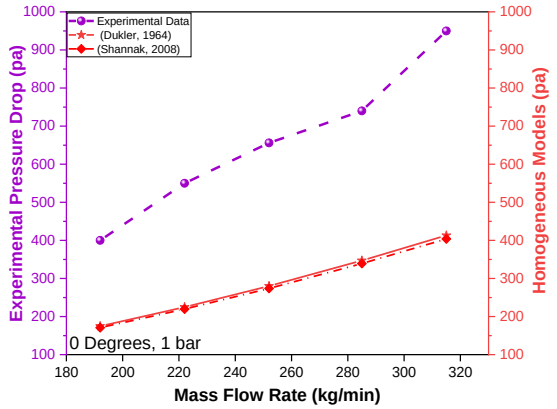
Experimental Data
(Dukler, 1964)
(Shannak, 2008)
Experimental Pressure Drop (pa)
Homogeneous Models (pa)
0 Degrees, 1 bar
Mass Flow Rate (kg/min)

(b)

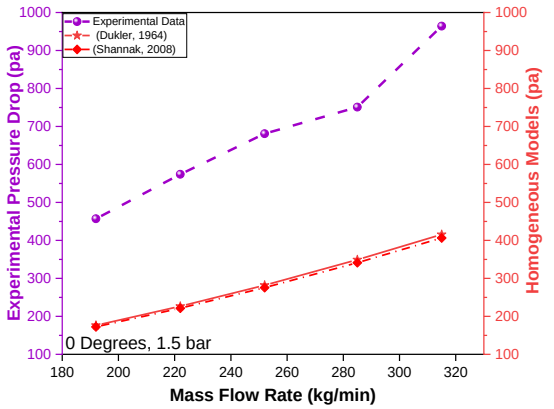
Experimental Data
(Dukler, 1964)
(Shannak, 2008)
Experimental Pressure Drop (pa)
Homogeneous Models (pa)
0 Degrees, 1.5 bar
Mass Flow Rate (kg/min)

(c)

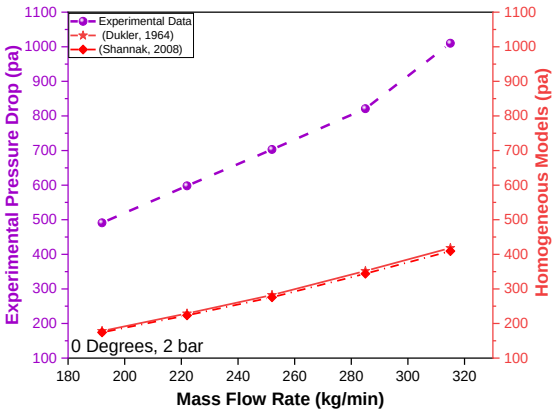
Experimental Data
(Dukler, 1964)
(Shannak, 2008)
Experimental Pressure Drop (pa)
Homogeneous Models (pa)
0 Degrees, 2 bar
Mass Flow Rate (kg/min)

(d)

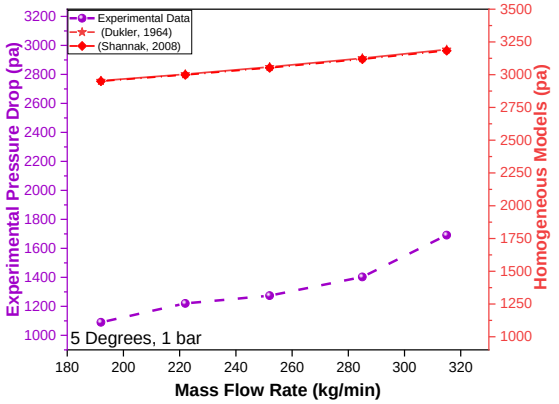
Experimental Data
(Dukler, 1964)
(Shannak, 2008)
Experimental Pressure Drop (pa)
Homogeneous Models (pa)
5 Degrees, 1 bar
Mass Flow Rate (kg/min)

(e)

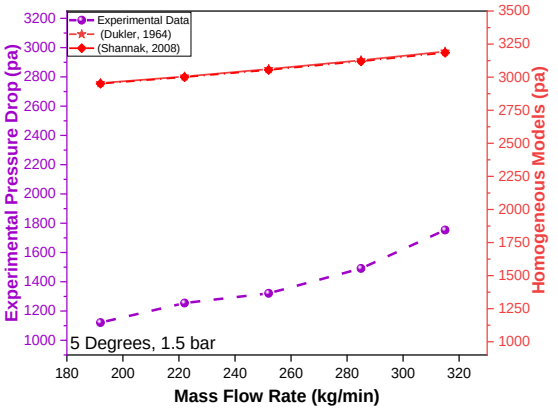
Experimental Data
(Dukler, 1964)
(Shannak, 2008)
Experimental Pressure Drop (pa)
Homogeneous Models (pa)
5 Degrees, 1.5 bar
Mass Flow Rate (kg/min)

(f)

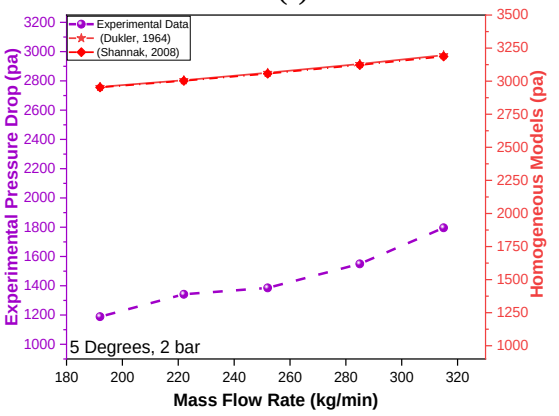
Experimental Data
(Dukler, 1964)
(Shannak, 2008)
Experimental Pressure Drop (pa)
Homogeneous Models (pa)
5 Degrees, 2 bar
Mass Flow Rate (kg/min)

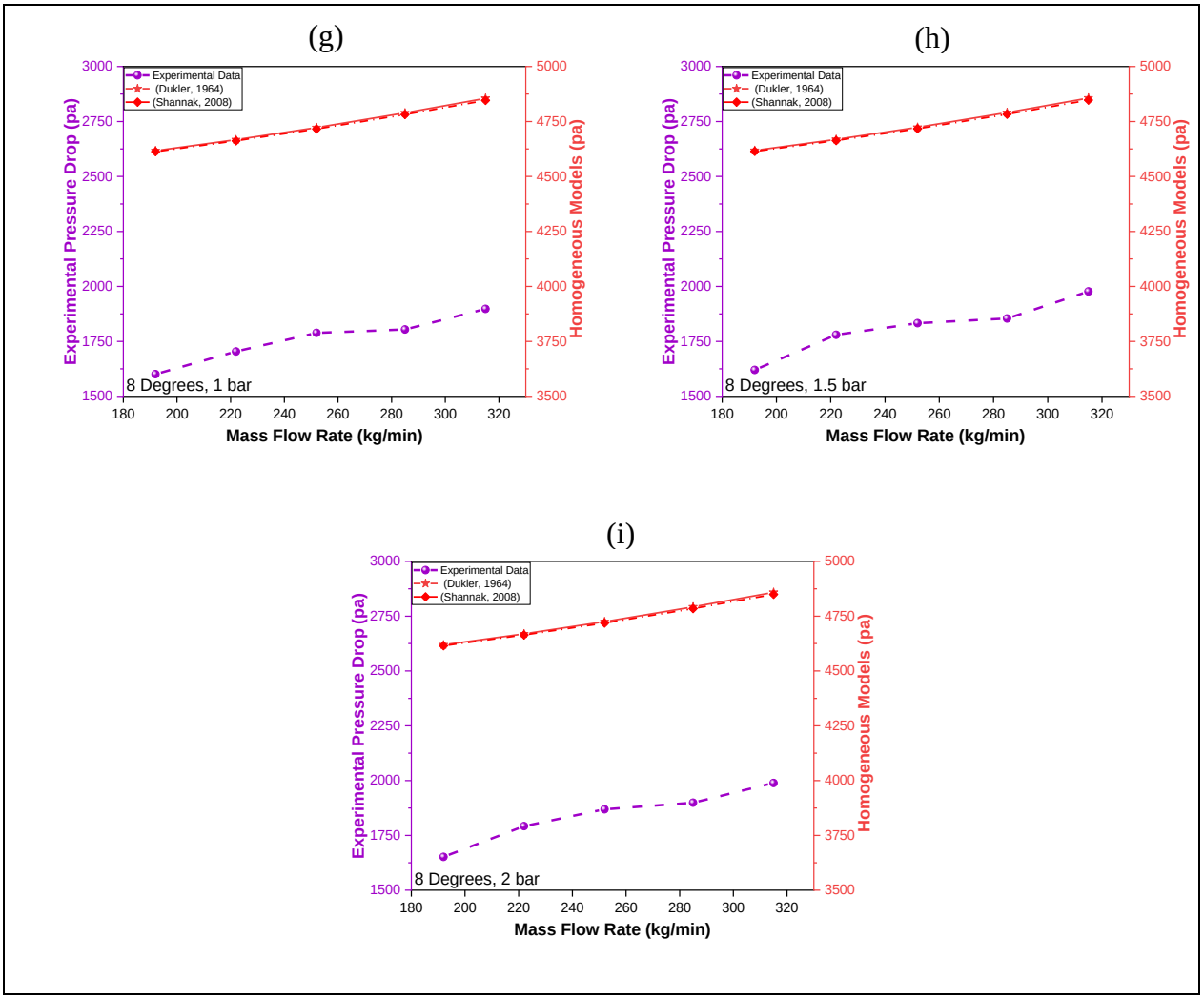

Figure 28: Comparing the experimental pressure drop data with Dukler's and Shannak's homogenous theoretical models at 0, 5, and 8 degrees with gas injection pressure of 1, 1.5 and 2 bars.

Figure 29 presents a comparison between the experimental pressure drop data and Lockhart-Martinelli's separated model at 0, 5, and 8 degrees with gas injection pressure of 1, 1.5 and 2 bars.

At the inclination of 0 degrees, both of the measured data and the separated model have an increasing trend with respect to the liquid mass flow rate. Speaking of the pressure drop, it can be noticed that there is a variation between the measured data and the

Lockhart-Martinelli's separated model, as the average pressure drop variations are 364.2 Pa, 382.7 Pa, and 415.9 Pa for 1, 1.5 and 2 bars. Also, it can be observed that at 0 degrees, the separated model underestimates the pressure drop.

Speaking of the impact of the injection pressure, the same conclusion that was made in the homogenous model can be applied here, as the separated model approach underestimates the influence of increasing the injection pressure. Taking the first point as an example, for the injection pressure of 1,1.5, and 2 bars at a constant liquid flow rate of 192 kg/min, the measured pressure drops were 400 Pa, 457 Pa and 491 Pa, while the pressure drops of Lockhart-Martinelli's separated model pressure drops are 172.7 Pa, 176 Pa, and 178.4 Pa.

As shown from Figure 29d to Figure 29f, it can be noticed that the variation between the measured data and Lockhart-Martinelli's separated model is huge. In the case of 5 degrees, and in contrast with the previous case of 0 degrees, Lockhart-Martinelli's separated model overestimated the measure pressure drop values for all cases of 1, 1.5, and 2 bars. The absolute average variations are 1740 Pa, 1693 Pa, and 1635 Pa for the injection pressure of 1,1.5, and 2 bars. The increase of the variations indicates that the Lockhart-Martinelli's separated model cannot accurately account for the increase of the inclination angles in annular cross-sectional pipes.

At 8 degrees of inclination, and similar to the case of 5 degrees, Lockhart-Martinelli's separated model overestimated the experimental pressure drop. It can be observed that as the inclination increases the error in the response of the pressure drop increases, as in comparison with the cases of 0 and 5 degrees, the 8 degrees inclination results in the

highest pressure drop variations.

Although there was a moderate variation between the experimental and theoretical values in the pressure drop in the case of 0 degrees, the model overestimated the actual pressure drop at higher inclinations. The Lockhart-Martinelli's separated model approach that was developed for the circular pipes, failed to predict the pressure drop through annular cross-sectional tube after the employment of the hydraulic diameter.

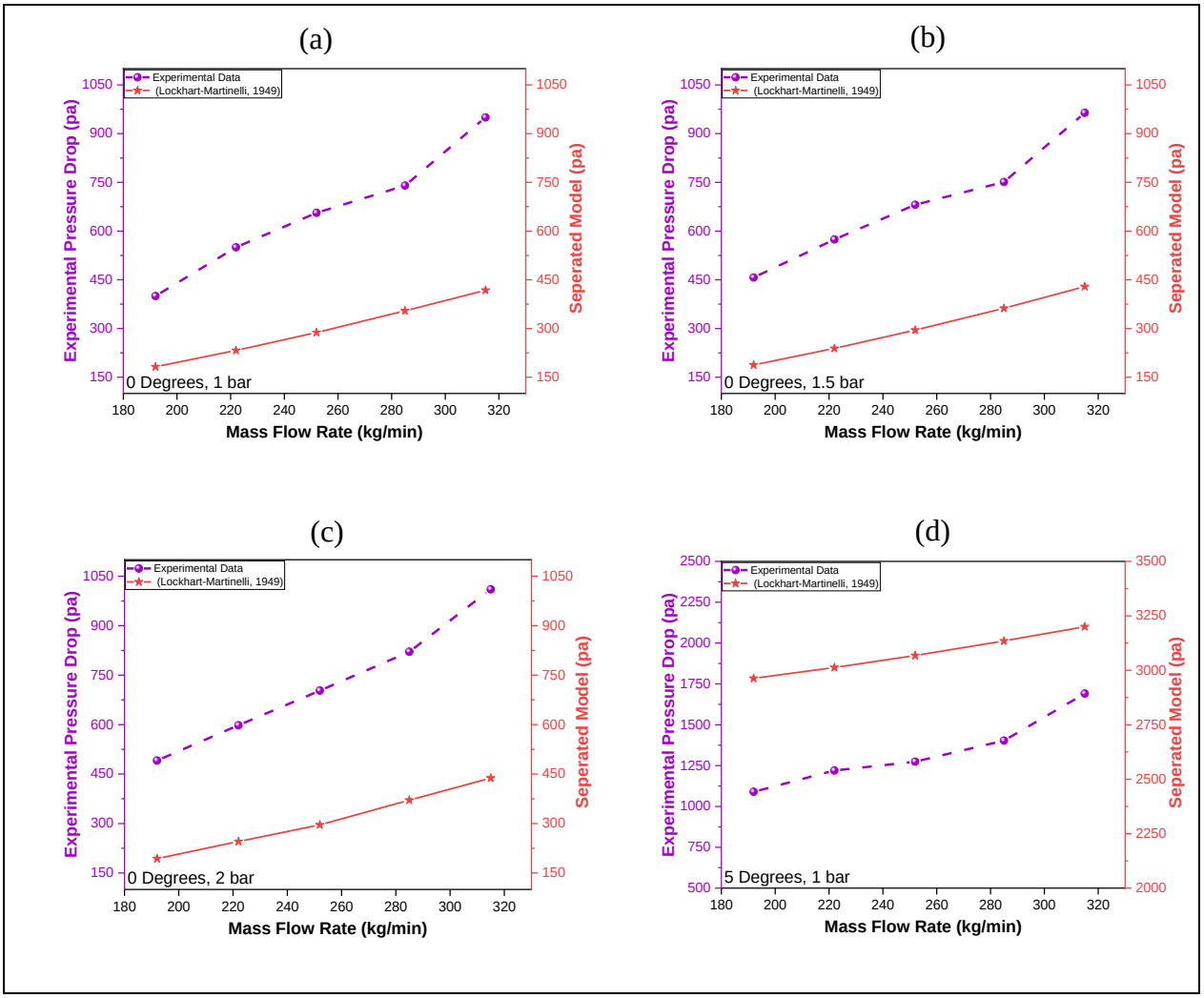

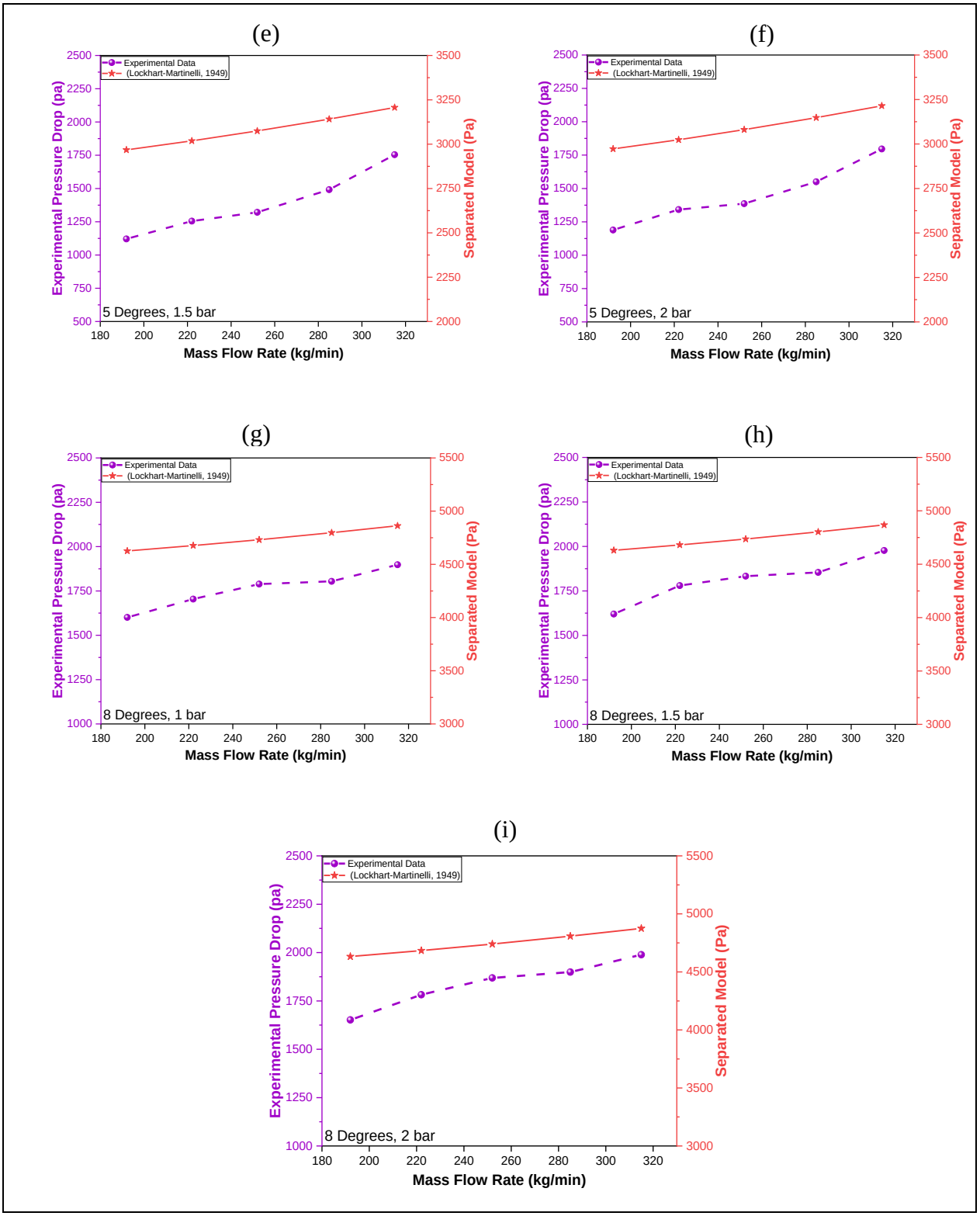

Figure 29: Comparing the experimental pressure drop data with Lockhart-Martinelli's separated model at 0, 5, and 8 degrees with gas injection pressure of 1, 1.5 and 2 bars.

Figure 30 presents a comparison between the experimental pressure drop data with Beggs and Brill theoretical model at 0, 5, and 8 degrees with gas injection pressure of 1, 1.5 and 2 bars

In Figure 30a, both of the measured data and Beggs and Brill theoretical model have an increasing trend with respect to the liquid mass flow rate. The same behavior can be observed in Figure 30b and Figure 30c. In terms of the pressure drop, it can be noticed that there is a low variation between the measured data and the theoretical model, as predicted values using the Beggs and Brill theoretical model are close to the actual pressure drop for gas injection pressure of 1, 1.5 and 2 bars. The average pressure drop variations are 147 Pa, 139 Pa, and 160 Pa for 1, 1.5 and 2 bars.

In the case of 5 degrees of inclination, it can be noticed that the variation between the measured data and Beggs and Brill theoretical model is larger than the case of 0 degrees, as the absolute average variations are 396 Pa, 372.4 Pa, and 338 Pa for the injection pressure of 1,1.5, and 2 bars. In comparison with the cases of 0 and 5 degrees, increasing the inclination to 8 degrees resulted in the highest pressure drop variations. At the inclination angle of 8 degrees and for the injection pressure of 1,1.5, and 2 bars, the variations between the measured data and the pressure drop models are 502.6 Pa, 493 Pa, and 499.2 Pa.

In contrast with the Homogenous and Lockhart-Martinelli's separated models, Beggs and Brill correlation has better pressure drop predictions and is considered to be more reliable than the Homogenous and Lockhart-Martinelli's separated models in annular tubes. However, in all inclination angles, Beggs and Brill correlation still overestimates

the actual pressure drop and do not accurately account for varying the angle of inclinations, liquid flow rates, and gas injection pressure for annular tubes.

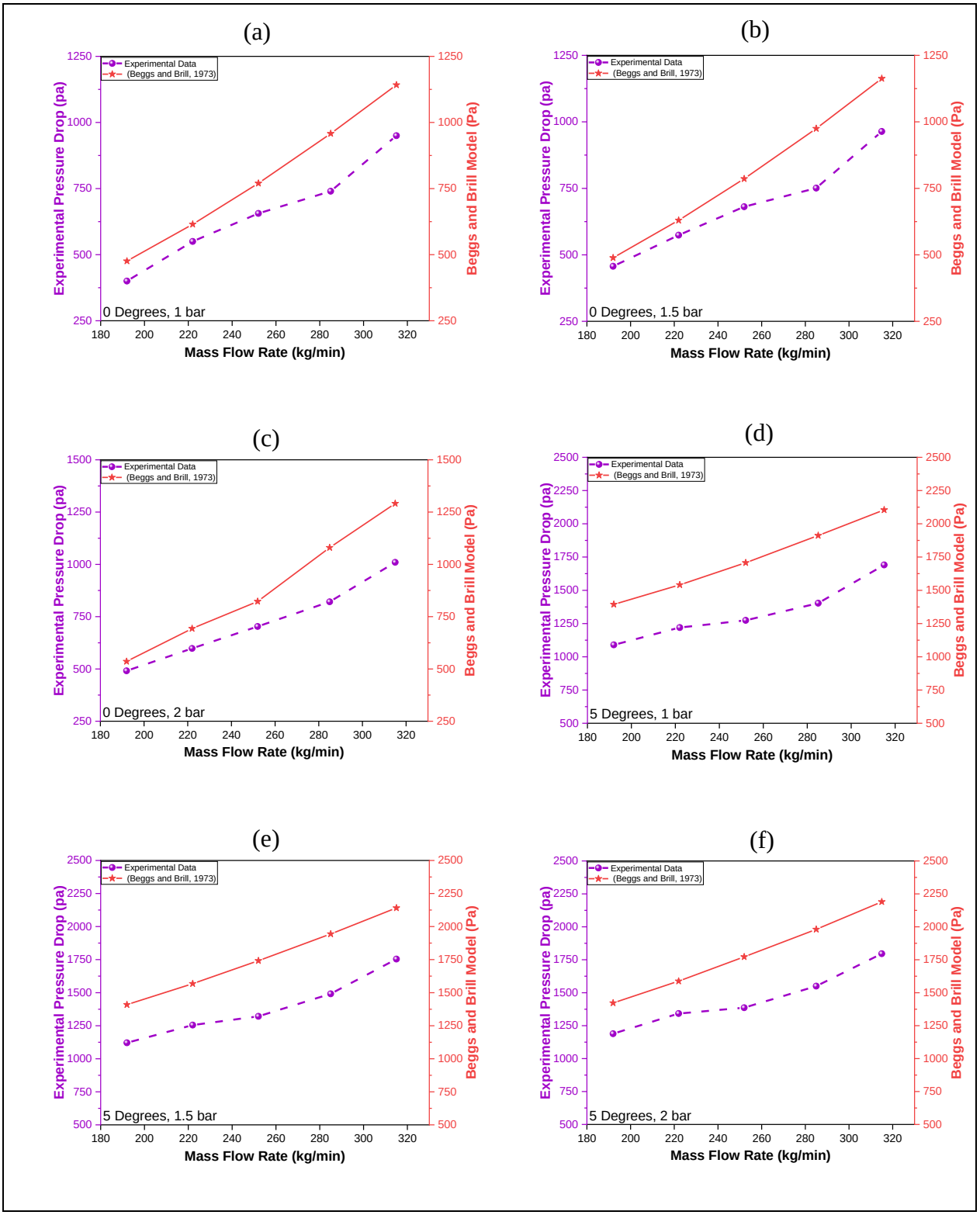

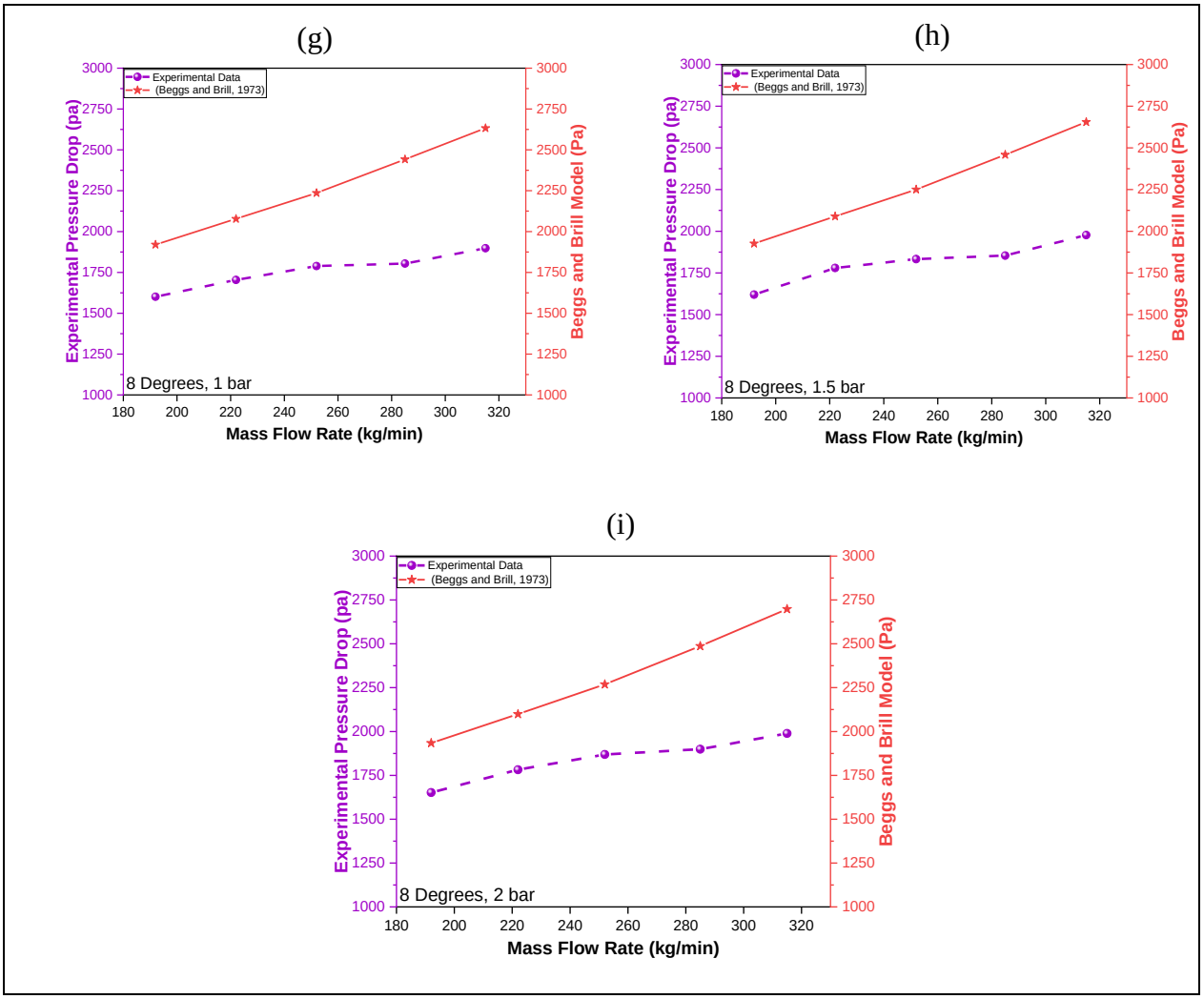

Figure 30: Comparing the experimental pressure drop data with Beggs and Brill theoretical model at 0, 5, and 8 degrees with gas injection pressure of 1, 1.5 and 2 bars.

4.4 Two-Phase Flow (Flowzan-Air)

Several experiments have been conducted using Flowzan as the liquid phase instead of water with a concentration of 0.15%. The flowrates, angle of inclination, and pressure injection pressure were varied. The same conditions were applied as the case of Water-Air flow. The experimental pressure drop results were used to evaluate various theoretical models. The theoretical models that were used in the case of Flowzan-Air flow are Dukler's and Shannak's homogeneous models, Lockhart-Martinelli's separated model, along with Beggs & Brill model.

Figure 31 presents a comparison between the experimental pressure drop data for Flowzan-Air flow and the theoretical models at 0, 5, and 8 degrees with gas injection pressure of 1, 1.5 and 2 bars.

For Dukler's and Shannak's homogenous models, at the inclination angle of 0 degrees, both models underestimate the entire range of the actual pressure drop. Nevertheless, in the cases of 5 and 8 degrees some predictions are overestimated while others are underestimated. At 0 degrees, it can be noticed that the predicted results of Shannak's are a bit closer to the measured pressure drop values compared to Dukler's model. However, both of models poorly describe the behavior of the actual pressure drop, and that can be clearly observed in Figure 31b and Figure 31c where the prediction values are more like a horizontal line.

For Lockhart-Martinelli's separated model, at the inclination angle of 0 degrees, the model underestimates the entire range of the actual pressure drop. And similar to the homogenous model, poor representation of the behavior can be noticed. Another thing

can be concluded here is that at higher viscosities, both of the homogenous and separated models do not accurately account for the increase of injection pressure and liquid flow rates, and this inaccuracy is clearly illustrated in the figures.

The Beggs and Brill model has the same increasing trend as the measured ones as shown from Figure 31g to Figure 31i. The model overestimates the measured pressure drop in the case of 0 degrees, but underestimates it in the cases of 5 and 8 degrees. Moreover, from the figures it is illustrated that the Beggs and Brill model has a better behavior representation when compared to homogenous and separated models.

In terms of pressure drop predictions, the Beggs and Brill model is considered the best theoretical pressure drop predictor, because as shown in the figures the pressure drop variations are lower in all cases of 0, 5 and 8 degrees when compared to Dukler's and Shannak's homogenous models and Lockhart-Martinelli's separated model. For Beggs and Brill model, the average pressure drop variations in the case of 0 degrees is 485.1 Pa, and it increases to 1067 Pa and 1680.6 Pa at 5 and 8 degrees, respectively. Despite that this model has a better curve representation, still the variations increase almost to double when the angle was increased.

In all models, a common thing that can be noticed is that at higher angles of inclination the behavior of the curves tends to be worse in describing the actual trend of pressure drop. That is due to the fact that the theoretical models poorly account for the effect of varying the angle of inclinations. That can be clearly seen in the predictions pressure drop values of Dukler's and Shannak's homogenous models and Lockhart-Martinelli's separated model for the cases of 5 and 8 degrees.

Despite the fact that the Beggs and Brill model can more or less predict the increasing behavior of experimental the pressure drop, more enhancements and developments should be done towards the concept of hydraulic diameter in annular tubes to accurately account for the variation of injection pressure, inclination angles and gas injection pressure.

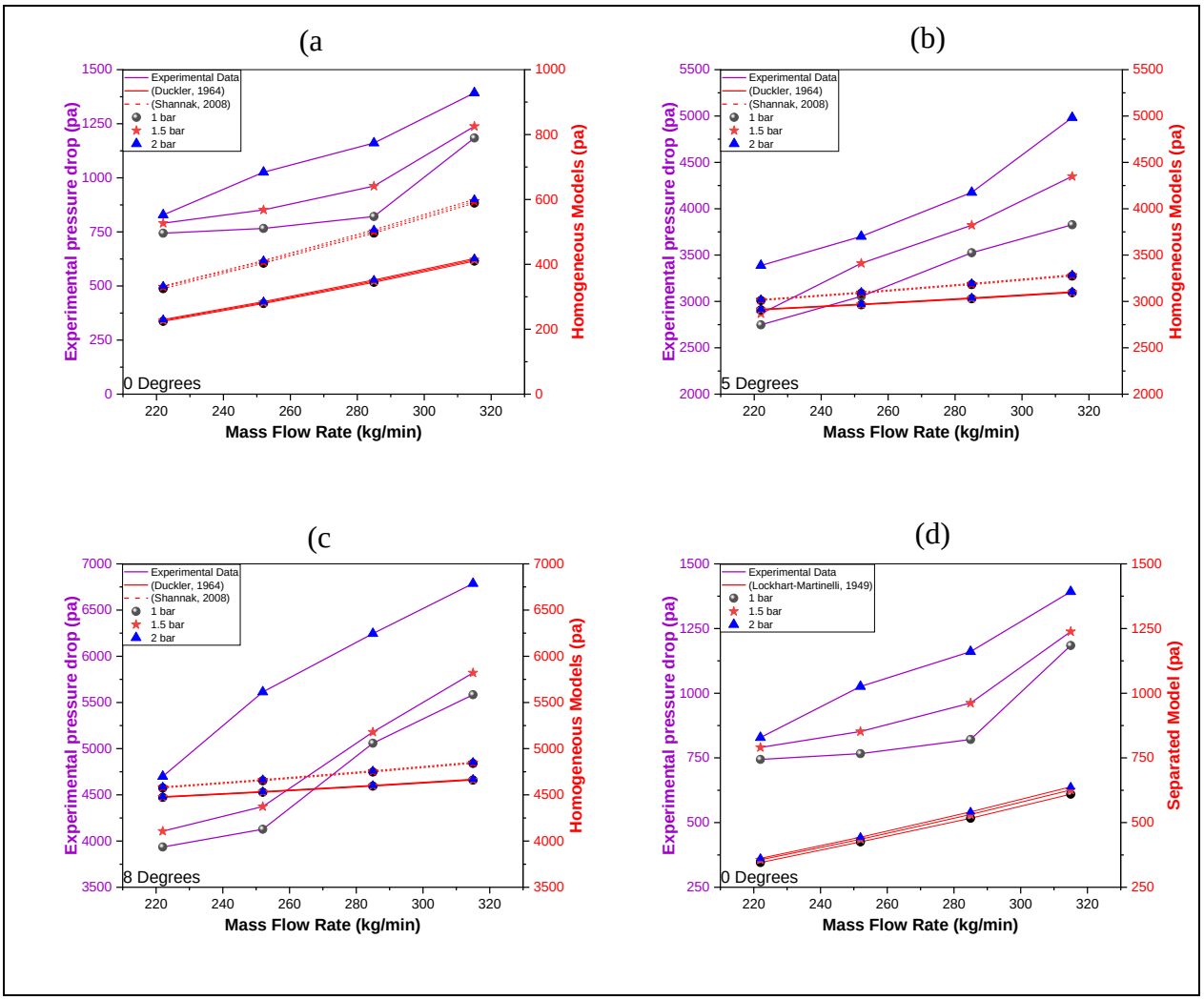

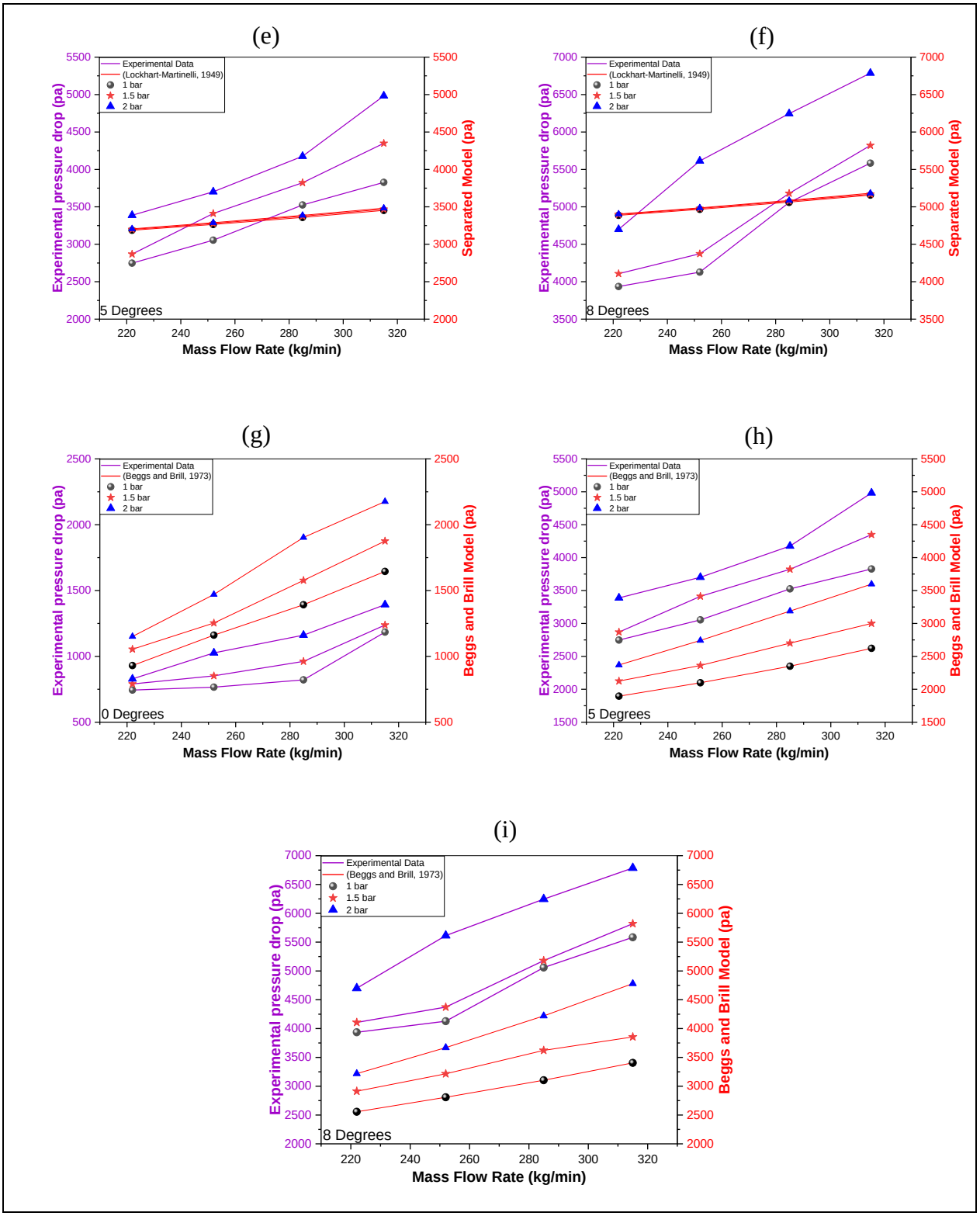

Figure 31: Comparing the experimental pressure drop data for Flowzan-Air two-phase flow with theoretical models at 0, 5, and 8 degrees with gas injection pressure of 1, 1.5 and 2 bars.

4.5 Correlation development

The statistical analysis is a powerful tool that is being used to accurately investigate the trends, patterns, and relationships of quantitative data. This method has been used to design and develop a mathematical correlation mainly for a two-phase liquid-gas flow through annular cross-sections. The experimental results conducted in Texas A&M university at Qatar have been used to develop this correlation by minimizing the least square error. It is worth mentioning that for a wider range of data, a better accuracy can be achieved by using the classical Bernoulli's correlation specially for higher angles of inclination. However, since the maximum angle that has been used in the lab was just 8 degrees, the error will not be evident in the developed correlation.

From Figure 32, it can be noticed that the majority of the predicted experimental pressure drop values fall in the error range of $\pm 13\%$. The constants of the developed correlation and the range of applicability are presented in Table 8 and Table 9. The developed power law correlation is expressed as:

$$\Delta P \,/\mathrm{L} = a Q_l^b \mathrm{U}_g^c Re^d \cos(\theta) \tag{61}$$

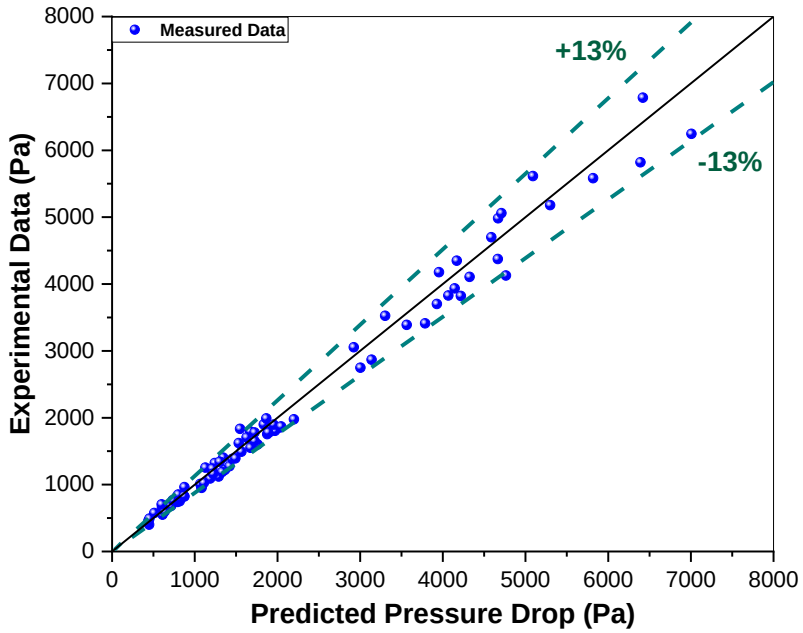

Figure 32: The range of error between the experimental data and the developed model

Table 8: Constants of the developed correlations

Constants	Value	Constants	Value
a	0.24	b	1.36
c	0.52	d	0.213

Table 9: Range of applicability

Limitations of the correlation	
Pump rotational speed (RPM)	700-1100
Liquid flow rate (kg/min)	192-315
Inclination angle (from horizontal)	0-8 degrees
Air injection Pressure	1-2 bars

4.6 Computational Fluid Dynamics

A numerical simulation was performed on an annular horizontal and near horizontal pipe. During model development, the coupled SIMPLE algorithm was employed to define the pressure velocity coupling. For the spatial discretization, the face value of variables was interpolated using the second order upwind scheme.

4.6.1 Multiphase Model

Eulerian-Eulerian multiphase model was applied since this approach computes momentum and continuity equations separately for liquid and gas phases. A conservation and energy balance equations of mass and momentum were utilized in this model.

The coupled between the phases was obtained through the initial predictions of pressure and interfacial terms. The continuity equations for liquid and gas are shown in Equations (62) and Equation (63) and momentum equations are shown in Equation (64) and Equation (65) respectively.

Continuity equation for liquid

$$\frac{\partial(\alpha_l \rho_l)}{\partial t} + \nabla.(\alpha_l \rho_l \vec{v}_l) = 0 \tag{62}$$

Continuity equation for gas

$$\frac{\partial(\alpha_g \rho_g)}{\partial t} + \nabla.(\alpha_g \rho_g \vec{v}_g) = 0 \tag{63}$$

Momentum equation for liquid

$$\frac{\partial(\alpha_l \rho_l \vec{v}_l)}{\partial t} + \nabla.(\alpha_l \rho_l \vec{v}_l \vec{v}_l) = -\alpha_l \nabla \mathrm{P} + \nabla.\left[\alpha_l \mu_{e,l}(\nabla \vec{v}_l - \nabla \vec{v}_l^T)\right] + \vec{F}_{IF} + \alpha_l \rho_l \mathrm{g} \quad (64)$$

Momentum equation for gas

$$\frac{\partial(\alpha_g \rho_g \vec{v}_g)}{\partial t} + \nabla.(\alpha_g \rho_g \vec{v}_g \vec{v}_g) = -\alpha_g \nabla \mathrm{P} + \nabla.\left[\alpha_g \mu_{e,g}(\nabla \vec{v}_g - \nabla \vec{v}_g^T)\right] + \vec{F}_{IF} + \alpha_g \rho_g \mathrm{g} \quad (65)$$

4.6.2 Turbulence Model

The prediction of turbulence in a multiphase phase flow is complex. The situation even gets worse in the case of liquid and gas due to the continues phase characteristics. On this work, the shear stress transport (SST) model will be utilized. This model is very accurate as it is known to be a hybrid model that combines both advantages of the bulk model and model near the wall.

For accurate predictions, the interphase forces will be taken into consideration while simulating the two-phase model. The total interphase force can be expressed as shown in Equation (66).

$$\vec{F}_{IF} = \vec{F}_{DF} + \vec{F}_{LF} + \vec{F}_{WF} \quad (66)$$

Where, $\vec{F}_{DF}$ is the drag force, $\vec{F}_{LF}$ is the lift force, and $\vec{F}_{WF}$ is the wall lubrication force.

1) Drag force

This force describes the resistive motion of the gas offered by the surrounding continuous liquid. In this force, the Grace model was applied. The Grace model accounts for both of the spherical and non-spherical geometries.

The drag force is expressed in Equation (67):

$$\vec{F}_{DF} = C_D(\frac{\pi}{4} * d_b^2 * \frac{\rho_l}{2})(\vec{v}_g - \vec{v}_l) \quad (67)$$

2) Lift force

The lift force plays a significant role in gas distribution, as it resolves the transverse forces resulted from vortex effect and velocity gradient while the particle is flowing in a shear flow. The lift force is expressed in Equation (68):

$$\vec{F}_{LF} = -C_L \rho_l \alpha_g (\vec{v}_g - \vec{v}_l) \times (\nabla \times \vec{v}_l) \quad (68)$$

3) Wall Lubrication Force

This force offers hydrodynamic pressure difference and computes the interaction between the gas and the wall. This correlation is valid for particles in both high and low viscosity systems.

$$\vec{F}_{WF} = C_{WL} \alpha_g \rho_l \left(v_g - v_l\right)^2 \vec{n}_{wall} \quad (69)$$

The coefficients C_{WL} and C_w can be expressed as the following:

$$C_{WL} = C_w \max\left(0, \frac{1}{C_{wd}} * \frac{1 - \frac{y_m}{C_{wc} d_b}}{y_w \left(\frac{y_w}{C_{wc} d_b}\right)}\right) \tag{70}$$

$$C_w = \max\left(\frac{7}{Re_b^{1.9}}, 0.0217(E_o)\right) \tag{71}$$

4.6.3 Validation of the Developed Model

ANSYS was used to simulate the two-phase gas-liquid flow for both Air-Water and Air-0.15% Flowzan. Figure 33 indicate that there is a good agreement between the experimental and computational results. The prediction of pressure drop results in $\pm 10\%$ error with measured pressure drop.

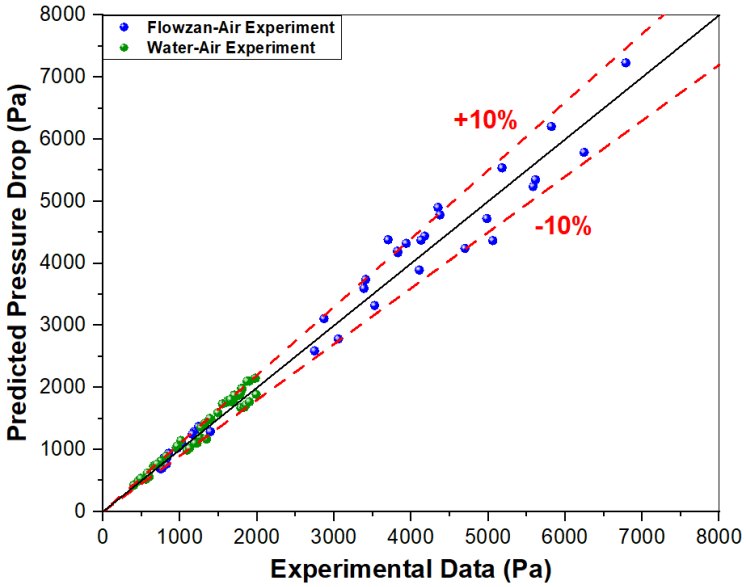

Figure 33: Validation of the computational model for Water-Air and Flowzan-Air experiments at 0, 5, and 8 degrees with gas injection pressure of 1, 1.5 and 2 bars.

4.6.4 Model Comparison with Theoretical Models

The developed two-phase CFD model has been used to predict the actual pressure drop values. The behavior of the model was then compared with multiple theoretical models. As illustrated in Figure 34, several predictions in both of Dukler's homogenous model and Lockhart-Martinelli's separated model were way out of the $\pm 40\%$ range. From the figure it can be noticed that at lower pressure drop values, Dukler's and Lockhart-Martinelli's models predictions underestimate the actual pressure drop values. However, the models started to overestimate the actual pressure drop data at higher values. In addition, both models poorly simulate the behavior of the actual pressure drop values. The absolute average relative errors for Dukler's and Lockhart-Martinelli's models are 74% and 81%, respectively.

Better behavior representation and predictions were observed by using Beggs and Brill model, as most of calculated pressure drop were located in the region of $\pm 40\%$, with an absolute average relative error of 29.17%. On the other hand, with regard to the developed two-phase CFD model, the majority of the predicted experimental pressure drop data falls in the error range of $\pm 10\%$, with an absolute relative error of 8.4%. Not to mention, beside the Beggs and Brill correlation, CFD predictions perform the best in simulating the behavior of the actual data.

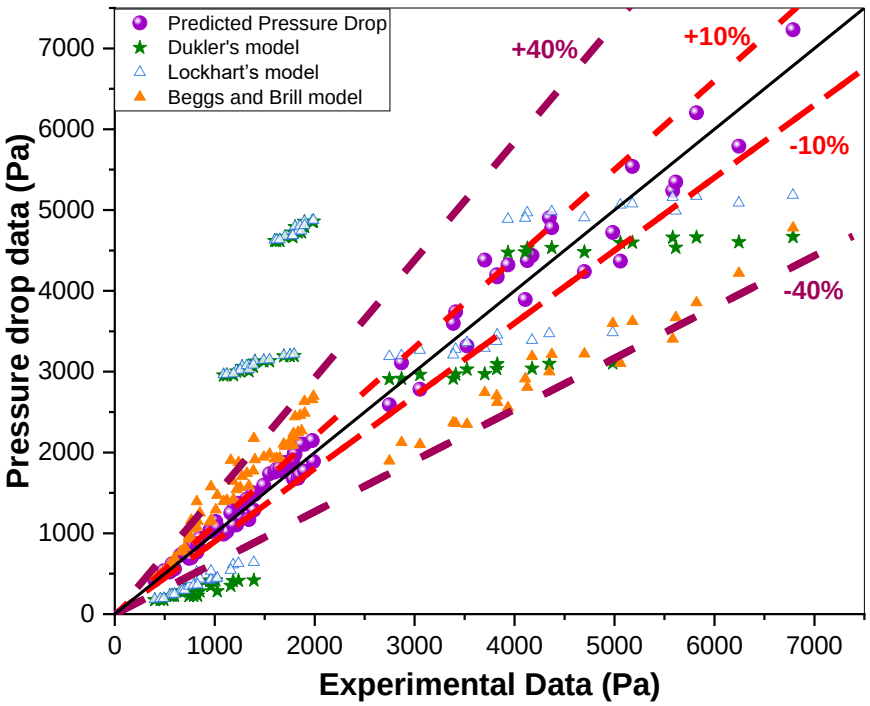

Figure 34: Comparison between different pressure models using Water-Air and Flowzan-Air combinations at 0, 5, and 8 degrees with gas injection pressure of 1, 1.5 and 2 bars.

CHAPTER 5: CONCLUSIONS AND FUTURE WORK

In this chapter, the main conclusions are given and discussed including those concluded from experimental work, CFD modeling and comparisons with available correlations. Then, the future direction of the research has been discussed, and some additional work has been proposed to further investigate the multiphase flow in annular geometries.

5.1 Conclusions

Multiple experiments have been conducted for single- and two-phase flow in TAMUQ flow loop system. The test rig was first calibrated by verifying the respective outputs of two dynamic pressure sensors attached to the data acquisition. In single phase flow experiments, the repeatability test was performed to ensure the system is repeatable.

In the two phase-flow experiments, both of Water-Air and 0.15%Flowzan-Air were used. Various theoretical two-phase flow correlations were compared with the measured data. A remarkable error was found between the actual pressure drop and the theoretical predictions for pressure drop in annular tubes.

After that, Ansys Workbench was used to simulate a two-phase flow case. Finally, the accuracy of the computational model in accounting for the liquid flow rate, inclination, and gas injection pressure has been examined by comparing it with the actual results along with theoretical models. The following are the main conclusions of this research:

1) The measured data from the flow loop system is considered to be repeatable and reproducible, as the repeatability test showed that the closeness of agreement between the results of successive measurements is as high as $\cong 98.64\%$.
2) For the single-phase flow, a good agreement between the experimental results and the theoretical model available in the literature with a maximum error of

3.9%. Thus, it is justified that the implementation of the hydraulic diameter will result in accurate predictions for the single-phase flow.

3) For two-phase flow experiments, Dukler's, Shannak's homogenous models, and Lockhart-Martinelli's separated model over- and underestimated the majority of the experimental pressure drop. Not to mention their poor response when accounting for the increase of injection pressure and angle of inclination. Beggs and Brill model performed the best among the theoretical models.
4) Dukler's homogenous model and Lockhart-Martinelli's separated model performed poorly with absolute relative errors of 74% and 81%, respectively.
5) Beggs and Brill model predicted the results with an absolute average relative error of 29.17% and was better than the rest of the theoretical model.
6) A two-phase computational fluid dynamic model was developed using Eulerian-Eulerian as the multiphase flow model and shear stress transport (SST) as the turbulence model, and the same experimental conditions and tube geometries were applied.
7) The majority of the prediction of pressure drop results were in the $\pm 10\%$ error range with respect to the measured pressure drop.
8) The accuracy of the developed computational model in accounting various parameters has been evaluated and compared with multiple theoretical correlation. The model performs the best in predicting the pressure drop with an absolute relative error of 8.4%.
9) A valid computational fluid dynamic model and approach have been developed in this thesis which serve as a reference for future research to predict pressure drop characteristics for two-phase flow in annular geometries within an error range of 10%.

5.2 Recommendations for Future Work

Although an extensive study has been done for single water flow in addition to the use of two different types of two-phase flow in annulus cross-sectional tube, one may perform some additional work for further investigations as the following:

1) More experimental work can be conducted by using a rotating inner rod to improve the prediction of pressure drop. Including the effect of the rotating inner pipe will enhance the accuracy of the developed model when compared with industrial field data, because in most cases the inner pipe of the annular tube is rotating specially in oil and gas exploration processes.
2) Study the effect of varying the viscosity by using other various types of industrial muds, other than the Flowzan.
3) Make some adjustments and modifications on the available flow loop system by adding some fittings, like elbows, and study the impact of these adjustments with respect to the pressure drop.
4) Investigate the characteristics of flow patterns/regimes in the annular tubes and make some conclusions by comparing it with some of the available theoretical models and maps to see if some improvements are required like the case of pressure drop.
5) The effect of adding solid particles can also be investigated and explored by conducting three-phase flow Air-Liquid-Solid experiments with varying the rotational speed of the inner pipe. That way, a complete simulation of the actual case will be achieved, because in reality there will be some rocks (solid phase) along with the liquid and gas phases.

REFERENCES

[1] G. F. Hewitt, “TWO-PHASE FLOWS,” in *A-to-Z Guide to Thermodynamics, Heat and Mass Transfer, and Fluids Engineering*, Begellhouse. doi: 10.1615/AtoZ.t.two-phase_flows.

[2] F. de Kerret, I. Benito, C. Béguin, D. Pelletier, and S. Etienne, “Two-phase flow pattern recognition in a varying section based on void fraction and pressure measurements,” *IOP Conference Series: Earth and Environmental Science*, vol. 49, p. 052015, Nov. 2016, doi: 10.1088/1755-1315/49/5/052015.

[3] U.S. Energy Information Administration, “U.S. Most Consumed Energy Sources,” Oct. 2008.

[4] A. D. Hill and D. Zhu, “The Relative Importance of Wellbore Pressure Drop and Formation Damage in Horizontal Wells,” Jun. 2006. doi: 10.2118/100207-MS.

[5] El-Sherik, A. M. (2017). *Trends in oil and gas corrosion research and technologies production and transmission*. Woodhead publishing.

[6] A. K. Sleiti, G. Takalkar, M. H. El-Naas, A. R. Hasan, and M. A. Rahman, “Early gas kick detection in vertical wells via transient multiphase flow modelling: A review,” *Journal of Natural Gas Science and Engineering*, vol. 80, p. 103391, Aug. 2020, doi: 10.1016/j.jngse.2020.103391.

[7] A. K. Sleiti *et al.*, “Comprehensive assessment and evaluation of correlations for gas-oil ratio, oil formation volume factor, gas viscosity, and gas density utilized in gas kick detection,” *Journal of Petroleum Science and Engineering*, vol. 207, p. 109135, Dec. 2021, doi: 10.1016/j.petrol.2021.109135.

[8] A. Barooah *et al.*, “Investigation of Gas-Liquid Flow Using Electrical Resistance Tomography and Wavelet Analysis Techniques for Early Kick Detection,” Jun. 2021.

doi: 10.1115/OMAE2021-63725.

[9] Sujoy Kumar Saha, *Microchannel Phase Change Transport Phenomena*. 2015.

[10] M. M., "Two-Phase Flow," in *An Overview of Heat Transfer Phenomena*, InTech, 2012. doi: 10.5772/54291.

[11] V. A. Kurganov, "PRESSURE DROP, SINGLE-PHASE," in *A-to-Z Guide to Thermodynamics, Heat and Mass Transfer, and Fluids Engineering*, Begellhouse. doi: 10.1615/AtoZ.p.pressure_drop_single-phase.

[12] A. Bahadori, *Single-phase and Multiphase Flow in Natural Gas Production Systems*. 2014. doi: 10.1016/b978-0-08-099971-5.00003-9.

[13] M. Jerez-Carrizales, J. E. Jaramillo, and D. Fuentes, "Prediction of Multiphase Flow in Pipelines: Literature Review," *Ingeniería y Ciencia*, pp. 213–233, 2015, doi: 10.17230/ingciencia.11.22.10.

[14] John R. Fanchi, *Integrated Reservoir Asset Management*. Elsevier, 2010. doi: 10.1016/C2009-0-62240-6.

[15] A. Nayak and P. Kulkarni, "Debris bed hydrodynamics, convective heat transfer and dryout," in *Severe Accidents in Nuclear Reactors*, Elsevier, 2021, pp. 297–353. doi: 10.1016/B978-0-12-822304-8.00010-3.

[16] A. Hernández, "Multiphase flow," in *Fundamentals of Gas Lift Engineering*, Elsevier, 2016, pp. 81–126. doi: 10.1016/B978-0-12-804133-8.00003-8.

[17] *VDI Heat Atlas*. Berlin, Heidelberg: Springer Berlin Heidelberg, 2010. doi: 10.1007/978-3-540-77877-6.

[18] J. and T. J. Collier, "Convective Boiling and Condensation," 1994.

[19] P. K. Vijayan, A. K. Nayak, and N. Kumar, "Steady-state and transient analysis of two-phase natural circulation systems," in *Single-Phase, Two-Phase and Supercritical Natural Circulation Systems*, Elsevier, 2019, pp. 187–235. doi: 10.1016/B978-0-08-

102486-7.00005-6.

[20] Y. Faghri, *Transport Phenomena in Multiphase Systems, Elsevier*. 2006.

[21] G. Wallis, *One-dimensional two-phase flow*. 1969.

[22] R. McAdams, "Vaporization inside horizontal tubes- II-benzene–oil mixtures," *ASME*, 1942.

[23] R. Cicchitti, "Two-phase cooling experiments—pressure drop, heat transfer, and burnout measurements," 1960.

[24] P. B. Whalley, "Boiling, condensation, and gas-liquid flow," 1990.

[25] Dukler, A. E., Wicks, M., & Cleveland, R. G. (1964). Frictional pressure drop in two-phase flow: B. an approach through similarity analysis. AIChE Journal, 10(1), 44–51. https://doi.org/10.1002/aic.690100118

[26] Beattie, D. R. H., & Whalley, P. B. (1982). A simple two-phase frictional pressure drop calculation method. *International Journal of Multiphase Flow*, *8*(1), 83–87. https://doi.org/10.1016/0301-9322(82)90009-x

[27] Lin, S., Kwok, C. C. K., Li, R.-Y., Chen, Z.-H., & Chen, Z.-Y. (1991). Local frictional pressure drop during vaporization of R-12 through capillary tubes. *International Journal of Multiphase Flow*, *17*(1), 95–102. https://doi.org/10.1016/0301-9322(91)90072-b

[28] Awad, M. M., & Muzychka, Y. S. (2008). Effective property models for homogeneous two-phase flows. *Experimental Thermal and Fluid Science*, *33*(1), 106–113. https://doi.org/10.1016/j.expthermflusci.2008.07.006

[29] Shannak, B. A. (2008). Frictional pressure drop of gas liquid two-phase flow in pipes. *Nuclear Engineering and Design*, *238*(12), 3277–3284. https://doi.org/10.1016/j.nucengdes.2008.08.015

[30] W. Xu, “Evaluation of frictional pressure drop correlations for two-phase flow in pipes,” *Nuclear engineering and design*, vol. 253, 2012.

[31] C. Lockhart, “Proposed correlation of data for isothermal two-phase, two-component flow in pipes,” *Chemical Engineering Progress*, vol. 45, 1949.

[32] Christopher E. Brennen, *Fundamentals of Multiphase Flows*. 2005.

[33] D. Chisholm, “A theoretical basis for the Lockhart-Martinelli correlation for two-phase flow,” *International Journal of Heat and Mass Transfer*, vol. 10, 1967.

[34] K. Sun, ““Evaluation analysis of prediction methods for two-phase flow pressure drop in mini-channels,” *International journal of multiphase flow*, vol. 35, 2009.

[35] P. Zhang, “A unified mechanistic model for slug liquid holdup and transition between slug and dispersed bubble flows,” *International journal of multiphase flow*, vol. 29, 2003.

[36] S. M. Zivi, “Estimation of steady-state steam void-fraction by means of the principle of minimum entropy production,” *Journal of Heat Transfer*, vol. 86, 1964.

[37] S. L. Smith, “Void fractions in two-phase flow: a correlation based upon an equal velocity head model,” *Proceedings of the Institution of Mechanical Engineers*, vol. 184, 1969.

[38] V. VDI Heat Atlas, “Flow Patterns in Evaporator Tubes,” in *VDI Heat Atlas, VDI-buch*, 2010, pp. 796–800.

[39] A. E. Rohuani, “ Calculation of volume void fraction in a subcooled and quality region,” *International Journal of Heat and Mass Transfer*, pp. 383–393, 1970.

[40] Beggs, D. H., & Brill, J. P. (1973). A study of two-phase flow in inclined pipes. *Journal of Petroleum Technology*, *25*(05), 607–617. https://doi.org/10.2118/4007-pa

[41] P. B. Whalley, “Boiling, condensation, and gas-liquid flow,” 1990.

[42] O. P. and G. C. Bergelin, “Cocurrent Gas-Liquid Flow. I. Flow in Horizontal Tubes,”

in *Proc. Heat Transfer and Fluid Mechanics Inst.*, 1949, pp. 5–18.

[43] Kosterin S. I., "An Investigation of the Influence of Diameter and Inclination of a Tube on the Hydraulic Resistance and Flow Structure of GasLiquid Mixtures," *Izvest. Akad, Nauk*, pp. 1824–1830, 1949.

[44] L. Cheng and D. Mewes, Eds., *Advances in Multiphase Flow and Heat Transfer (Volume 3)*. BENTHAM SCIENCE PUBLISHERS, 2012. doi: 10.2174/97816080522881120101.

[45] M. L. Corradini, ""Multiphase Flow: Gas/Liquid," 1998.

[46] T. N. Wong and Y. K. Yau, "Flow patterns in two-phase air-water flow," *International Communications in Heat and Mass Transfer*, vol. 24, pp. 111–118, 1997.

[47] V. C. Kelessidis and A. E. Dukler, "Heat transfer measurements and correlations for air–water flow of different flow patterns in a horizontal pipe," *Experimental Thermal and Fluid Science*, vol. 15, pp. 173–191, 1989.

[48] C.-Y. Yang and C.-C. Shieh, ""Flow pattern of air–water and two-phase R-1 4a in small circular tubes," *International journal of multiphase flow*, vol. 27, pp. 1163–1177, 2001.

[49] P. L. Spedding and T. van Nguyen, "Regime maps for air water two phase flow," *Chemical Engineering Science*, vol. 35, pp. 779–793, 1980.

[50] J. M. Mandhane, G. A. Gregory, and K. Aziz, "A flow pattern map for gas—liquid flow in horizontal pipes," *International journal of multiphase flow*, vol. 1, pp. 537–553, 1974.

[51] D. Baker, "Simultaneous Flow of Oil and Gas," *Oil and Gas Journal* , vol. 53, pp. 183–195, 1954.

[52] G. E. Alves, "Cocurrent Liquid-Gas Flow in a Pipeline Contractor," *Chemical Engineering Progress*, vol. 50, pp. 449–456, 1954.

[53] P. L. Spedding and van Nguyen, “Regime maps for air water two phase flow,” *Chemical Engineering Science*, vol. 35, pp. 779–793, 1980.

[54] P. L. Spedding and D. R. Spence, “Flow regimes in two-phase gas-liquid flow,” *International journal of multiphase flow*, vol. 19, pp. 245–280, 1993.

[55] N. P. Hand and P. L. Spedding, “Horizontal gas-liquid flow at close to atmospheric conditions,” *Chemical Engineering Science*, vol. 48, pp. 2283–2305, 1993.

[56] K. Manikonda *et al.*, “Application of Machine Learning Classification Algorithms for Two-Phase Gas-Liquid Flow Regime Identification,” Dec. 2021. doi: 10.2118/208214-MS.

[57] K. Manikonda *et al.*, “Horizontal Two-Phase Flow Regime Identification with Machine Learning Classification Models,” Feb. 2022. doi: 10.2523/IPTC-22153-MS.

[58] M. Salcudean, D. C. Groeneveld, and L. Leung, “Effect of flow obstruction geometry on pressure drops in horizontal air-water flow,” *International journal of multiphase flow*, vol. 9, pp. 73–85, 1983.

[59] M. Salcudean, J. H. Chun, and D. C. Groeneveld, “Effect of flow obstruction on void distribution in horizontal air-water flow,” *International journal of multiphase flow*, vol. 9, pp. 91–96, 1983.

[60] A. R. Hasan and C. S. Kabir, “Two-phase flow in vertical and inclined annuli,” *International journal of multiphase flow*, vol. 18, pp. 279–293, 1992.

[61] S. I. Osamusali, “Study of gas-liquid two-phase flow pattern transitions in horizontal pipe, annulus and nuclear fuel type rod bundle flow systems,” 1988.

[62] S. I. Osamusali and J. Chang, “Two phase flow regime transition in a horizontal pipe and annulus flow under gas–liquid two-phase flow,” *ASME Fundamentals of Gas–Liquid Flows*, vol. 72, pp. 63–69, 1988.

[63] F. A. A. Mendes, O. M. H. Rodriguez, V. Estevam, and D. Lopes, “Flow patterns in

inclined gas-liquid annular duct flow," in *Computational methods in multiphase flow*, 2011, pp. 271–283.

[64] N. P. Ekberg, S. M. Ghiaasiaan, S. I. Abdel-Khalik, M. Yoda, and S. M. Jeter, "Gas–liquid two-phase flow in narrow horizontal annuli," *Nuclear engineering and design*, vol. 192, pp. 59–80, 1999.

[65] A. A. Sunthankar, E. Kuru, S. Miska, and A. Kamp, "New developments in aerated mud hydraulics for drilling in inclined wells," *SPE drilling & completion*, vol. 18, pp. 152–158, 2003.

[66] S. Wongwises and M. Pipathattakul, "Flow pattern, pressure drop and void fraction of two-phase gas–liquid flow in an inclined narrow annular channel," *Experimental Thermal and Fluid Science*, vol. 30, pp. 345–354, 2006.

[67] C. Omurlu, "Mathematical modeling of horizontal two-phase flow through fully eccentric annuli," 2006.

[68] R. E. Osgouei, M. E. Ozbayoglu, M. Ozbayoglu, and E. H. Yuksel, "The Determination of Two Phase Liquid-Gas Flow Behavior Through Horizontal Eccentric Annular Geometry by Modification of Beggs & Brill and Lockhart & Martinelli Models," *American Society of Mechanical Engineers*, 2013.

[69] D. A. Lote, V. Vinod, and A. W. Patwardhan, "Computational Fluid Dynamics Simulations of the Air-Water Two-Phase Vertically Upward Bubbly Flow in Pipes," *Industrial and Engineering Chemistry Research*, vol. 57, no. 31, pp. 10609–10627, Aug. 2018, doi: 10.1021/acs.iecr.8b01579.

[70] S. Sun, Z. Hou, J. Feng, and G. Yu, "Research on gas bubble formation using CFD during gas kick," *Integrated Ferroelectrics*, vol. 199, no. 1, pp. 179–192, Jun. 2019, doi: 10.1080/10584587.2019.1592612.

[71] R. A. Sultan, M. A. Rahman, S. Rushd, S. Zendehboudi, and V. C. Kelessidis,

"Validation of CFD model of multiphase flow through pipeline and annular geometries," *Particulate Science and Technology*, vol. 37, no. 6, pp. 685–697, Aug. 2019, doi: 10.1080/02726351.2018.1435594.

[72] R. A. Sultan, S. Alfarek, M. A. Rahman, and S. Zendehboudi, "CFD and experimental approach on three phase gas-liquid-solid newtonian fluid flow in horizontal pipes," *International Journal of Computational Methods and Experimental Measurements*, vol. 7, no. 1, pp. 33–44, 2019, doi: 10.2495/CMEM-V7-N1-33-44.

[73] G. S. Gray and S. J. Ormiston, "A Comparative Study of Closure Relations for CFD Modelling of Bubbly Flow in a Vertical Pipe," *Open Journal of Fluid Dynamics*, vol. 11, no. 02, pp. 98–134, 2021, doi: 10.4236/ojfd.2021.112007.

[74] G. F. Hewitt, "Multiphase fluid flow and pressure drop: Introduction and fundamentals," in *Heat Exchanger Design Handbook Chapter 2.3.1* , New York: Hemisphere Publishing Corporation.

APPENDIX A: NOMENCLATURE

Table 10: Nomenclature

symbol	Description	Unit
$u_{s,l}$	Liquid superficial velocity	m/s
$u_{s,g}$	Gas superficial velocity	m/s
$u_{s,m}$	Mixture superficial velocity	m/s
Q_l	Gas volumetric flowrate	m^3/s
Q_g	Liquid volumetric flowrate	m^3/s
A	Cross-sectional area	m^2
G	Mass flux	$kg.m^{-2}.s^{-1}$
ρ_l	Liquid density	kg/m^3
ρ_g	Gas density	kg/m^3
x	Mass quality	-
$\dot{M}_g$	Gas mass flow rate	kg/s
$\dot{M}_l$	Liquid mass flow rate	kg/s
β_q	volumetric quality	-
$Re_{s,l}$	Superficial liquid Reynolds number	-
$Re_{s,g}$	Superficial gas Reynolds number	-
D	Circular diameter	m
Re_{hom}	Homogeneous Reynolds number	-
μ_{hom}	Homogeneous viscosity	$N.s/m^2$
f	Friction factor	-
Δp	Pressure drop	Pa
μ_g	Gas dynamic viscosity	$N.s/m^2$
μ_l	Liquid dynamic viscosity	$N.s/m^2$
Δp_l	Liquid frictional pressure	Pa
Δp_g	Gas frictional pressure	Pa
α_{hom}	Homogeneous void fraction	-
ϕ_l^2	Liquid frictional multiplier	-
ϕ_g^2	Ga frictional multipliers	-
f_l	Liquid Friction factor	-

APPENDIX A: NOMENCLATURE, CONTINUED

symbol	Description	Unit
f_g	Gas Friction factor	-
S_v	Velocity ratio	-
g	Acceleration due to gravity	m/s^2
α_l	Liquid volume fraction	-
α_g	Gas volume fraction	-
$\vec{v}_l$	Liquid velocity vector	m/s
λ	Input liquid content	-
β	Input Gas content	-
G_m	Mixture mass flux	$kg.m^{-2}.s^{-1}$
S	Area of the channel	m^2
$\dot{V}_l$	Volume flow rate	m^3/s
ε_i	Mean phase content	-
ρ_H	Homogenous density	kg/m^3
$\dot{m}_l$	Mass flux of the ith phase	$kg.m^{-2}.s^{-1}$
τ_o	Wall shear stress	Pa
q	Wall heat	J
$\dot{q}$	Wall heat flux	W/m^2
$\dot{q}_v$	Internal heat generation rate	W/m^3
e	Energy converted per unit fluid mass	J/kg
h	Specific enthalpy	kJ/kg
z	Axial distance	m
$\mu_{e,g}$	Effective viscosity for gas	$N.s/m^2$
$\mu_{specific}$	Specific viscosity	$N.s/m^2$
Fr_H	Homogenous Froude number	-
S	Beggs and Brill Pressure drop factor	-
H_L	Liquid hold-up	-
d_h	Hydraulic diameter	m
y_w	Distance to the nearest wall	m
$\mu_{e,l}$	Effective viscosity for liquid	$N.s/m^2$

APPENDIX B: ONE-PHASE LIQUID EXPERIMENTS

Table 11: Single Phase Experiments Using Water at 0 Degrees

Exp.	Phase Flow	Working Fluid	Pump Speed	Mass Flow Rate	System pressure	Eccentricity	Inclination
-	-	-	(RPM)	(kg/min)	(bar)	(%)	(^{o})
1	One phase	Water	700	192	1	0	0
2	One phase	Water	800	222	1	0	0
3	One phase	Water	900	252	1	0	0
4	One phase	Water	1000	285	1	0	0
5	One phase	Water	1100	315	1	0	0

Table 12: Single Phase Experiments Using Water at 5 Degrees

Exp.	Phase Flow	Working Fluid	Pump Speed	Mass Flow Rate	System pressure	Eccentricity	Inclination
-	-	-	(RPM)	(kg/min)	(bar)	(%)	(^{o})
1	One phase	Water	700	192	1	0	5
2	One phase	Water	800	222	1	0	5
3	One phase	Water	900	252	1	0	5
4	One phase	Water	1000	285	1	0	5
5	One phase	Water	1100	315	1	0	5

Table 13: Single Phase Experiments Using Water at 8 Degrees

Exp.	Phase Flow	Working Fluid	Pump Speed	Mass Flow Rate	System pressure	Eccentricity	Inclination
-	-	-	(RPM)	(kg/min)	(bar)	(%)	(^{o})
1	One phase	Water	700	192	1	0	8
2	One phase	Water	800	222	1	0	8
3	One phase	Water	900	252	1	0	8
4	One phase	Water	1000	285	1	0	8
5	One phase	Water	1100	315	1	0	8

Table 14: Single Phase Experiments Using Flowzan at 0 Degrees

Exp.	Phase Flow	Working Fluid	Liquid Concentration	Pump Speed	Mass Flow Rate	System pressure	Eccentricity	Inclination
-	-	-	%	(RPM)	(kg/m)	(bar)	(%)	(^{o})
1	One phase	Flowzan	0.15	700	192	1	0	0
2	One phase	Flowzan	0.15	800	222	1	0	0
3	One phase	Flowzan	0.15	900	252	1	0	0
4	One phase	Flowzan	0.15	1000	285	1	0	0
5	One phase	Flowzan	0.15	1100	315	1	0	0

Table 15: Single Phase Experiments Using Flowzan at 5 Degrees

Exp.	Phase Flow	Working Fluid	Liquid Concentration	Pump Speed	Mass Flow Rate	System pressure	Eccentricity	Inclination
-	-	-	%	(RPM)	(kg/m)	(bar)	(%)	(^{o})
1	One phase	Flowzan	0.15	700	192	1	0	5
2	One phase	Flowzan	0.15	800	222	1	0	5
3	One phase	Flowzan	0.15	900	252	1	0	5
4	One phase	Flowzan	0.15	1000	285	1	0	5
5	One phase	Flowzan	0.15	1100	315	1	0	5

Table 16: Single Phase Experiments Using Flowzan at 8 Degrees

Exp.	Phase Flow	Working Fluid	Liquid Concentration	Pump Speed	Mass Flow Rate	System pressure	Eccentricity	Inclination
-	-	-	%	(RPM)	(kg/m)	(bar)	(%)	(^{o})
1	One phase	Flowzan	0.15	700	192	1	0	8
2	One phase	Flowzan	0.15	800	222	1	0	8
3	One phase	Flowzan	0.15	900	252	1	0	8
4	One phase	Flowzan	0.15	1000	285	1	0	8
5	One phase	Flowzan	0.15	1100	315	1	0	8

APPENDIX C: TWO-PHASE GAS-LIQUID EXPERIMENTS

Table 17: Two Phase Experiments Using Water-Air at 0 Degrees

Exp.	Phase Flow	Working Fluids	Mass Flow Rate	Gas Injection pressure	Eccentricity	Inclination	Pressure Drop
-	-	-	(kg/min)	(bar)	(%)	(^{o})	(Pa)
1	Two-phase	Air-Water	192	1	0	0	400
2	Two-phase	Air-Water	222	1	0	0	550
3	Two-phase	Air-Water	252	1	0	0	656
4	Two-phase	Air-Water	285	1	0	0	740
5	Two-phase	Air-Water	315	1	0	0	950
6	Two-phase	Air-Water	192	1.5	0	0	457
7	Two-phase	Air-Water	222	1.5	0	0	574
8	Two-phase	Air-Water	252	1.5	0	0	681
9	Two-phase	Air-Water	285	1.5	0	0	751
10	Two-phase	Air-Water	315	1.5	0	0	964
11	Two-phase	Air-Water	192	2	0	0	491
12	Two-phase	Air-Water	222	2	0	0	598
13	Two-phase	Air-Water	252	2	0	0	703
14	Two-phase	Air-Water	285	2	0	0	821
15	Two-phase	Air-Water	315	2	0	0	1010

Table 18: Two Phase Experiments Using Water-Air at 5 Degrees

Exp.	Phase Flow	Working Fluids	Mass Flow Rate	Gas Injection pressure	Eccentricity	Inclination	Pressure Drop
-	-	-	(kg/min)	(bar)	(%)	(^{o})	(Pa)
1	Two-phase	Air-Water	192	1	0	5	1090
2	Two-phase	Air-Water	222	1	0	5	1220
3	Two-phase	Air-Water	252	1	0	5	1274
4	Two-phase	Air-Water	285	1	0	5	1403
5	Two-phase	Air-Water	315	1	0	5	1691
6	Two-phase	Air-Water	192	1.5	0	5	1121
7	Two-phase	Air-Water	222	1.5	0	5	1255
8	Two-phase	Air-Water	252	1.5	0	5	1321
9	Two-phase	Air-Water	285	1.5	0	5	1491
10	Two-phase	Air-Water	315	1.5	0	5	1754
11	Two-phase	Air-Water	192	2	0	5	1189
12	Two-phase	Air-Water	222	2	0	5	1342
13	Two-phase	Air-Water	252	2	0	5	1386
14	Two-phase	Air-Water	285	2	0	5	1550
15	Two-phase	Air-Water	315	2	0	5	1796

Table 19: Two Phase Experiments Using Water-Air at 8 Degrees

Exp.	Phase Flow	Working Fluids	Mass Flow Rate	Gas Injection pressure	Eccentricity	Inclination	Pressure Drop
-	-	-	(kg/min)	(bar)	(%)	(^{o})	(Pa)
1	Two-phase	Air-Water	192	1	0	8	1601
2	Two-phase	Air-Water	222	1	0	8	1704
3	Two-phase	Air-Water	252	1	0	8	1789
4	Two-phase	Air-Water	285	1	0	8	1804
5	Two-phase	Air-Water	315	1	0	8	1898
6	Two-phase	Air-Water	192	1.5	0	8	1620
7	Two-phase	Air-Water	222	1.5	0	8	1780
8	Two-phase	Air-Water	252	1.5	0	8	1833
9	Two-phase	Air-Water	285	1.5	0	8	1854
10	Two-phase	Air-Water	315	1.5	0	8	1977
11	Two-phase	Air-Water	192	2	0	8	1652
12	Two-phase	Air-Water	222	2	0	8	1782
13	Two-phase	Air-Water	252	2	0	8	1869
14	Two-phase	Air-Water	285	2	0	8	1899
15	Two-phase	Air-Water	315	2	0	8	1989

Table 20:Two Phase Experiments Using Flowzan-Air at 0 Degrees

Exp.	Phase Flow	Working Fluids	Mass Flow Rate	Gas Injection pressure	Eccentricity	Inclination	Pressure Drop
-	-	-	(kg/min)	(bar)	(%)	(^{o})	(Pa)
1	Two-phase	Air-0.15% Flowzan	222	1	0	0	744
2	Two-phase	Air-0.15% Flowzan	252	1	0	0	766
3	Two-phase	Air-0.15% Flowzan	285	1	0	0	821
4	Two-phase	Air-0.15% Flowzan	315	1	0	0	1184
5	Two-phase	Air-0.15% Flowzan	222	1.5	0	0	791
6	Two-phase	Air-0.15% Flowzan	252	1.5	0	0	852
7	Two-phase	Air-0.15% Flowzan	285	1.5	0	0	962
8	Two-phase	Air-0.15% Flowzan	315	1.5	0	0	1238
9	Two-phase	Air-0.15% Flowzan	222	2	0	0	829
10	Two-phase	Air-0.15% Flowzan	252	2	0	0	1026
11	Two-phase	Air-0.15% Flowzan	285	2	0	0	1161
12	Two-phase	Air-0.15% Flowzan	315	2	0	0	1393

Table 21: Two Phase Experiments Using Flowzan-Air at 5 Degrees

Exp.	Phase Flow	Working Fluids	Mass Flow Rate	Gas Injection pressure	Eccentricity	Inclination	Pressure Drop
-	-	-	(kg/min)	(bar)	(%)	(^{o})	(Pa)
1	Two-phase	Air-0.15% Flowzan	222	1	0	5	2748
2	Two-phase	Air-0.15% Flowzan	252	1	0	5	3054
3	Two-phase	Air-0.15% Flowzan	285	1	0	5	3525
4	Two-phase	Air-0.15% Flowzan	315	1	0	5	3827
5	Two-phase	Air-0.15% Flowzan	222	1.5	0	5	2869
6	Two-phase	Air-0.15% Flowzan	252	1.5	0	5	3411
7	Two-phase	Air-0.15% Flowzan	285	1.5	0	5	3822
8	Two-phase	Air-0.15% Flowzan	315	1.5	0	5	4349
9	Two-phase	Air-0.15% Flowzan	222	2	0	5	3388
10	Two-phase	Air-0.15% Flowzan	252	2	0	5	3702
11	Two-phase	Air-0.15% Flowzan	285	2	0	5	4176
12	Two-phase	Air-0.15% Flowzan	315	2	0	5	4983

APPENDIX C: TWO-PHASE GAS-LIQUID EXPERIMENTS, CONTINUED

Table 22: Two Phase Experiments Using Flowzan-Air at 8 Degrees

Exp.	Phase Flow	Working Fluids	Mass Flow Rate	Gas Injection pressure	Eccentricity	Inclination	Pressure Drop
-	-	-	(kg/min)	(bar)	(%)	(^{o})	(Pa)
1	Two-phase	Air-0.15% Flowzan	222	1	0	8	3935
2	Two-phase	Air-0.15% Flowzan	252	1	0	8	4128
3	Two-phase	Air-0.15% Flowzan	285	1	0	8	5059
4	Two-phase	Air-0.15% Flowzan	315	1	0	8	5583
5	Two-phase	Air-0.15% Flowzan	222	1.5	0	8	4107
6	Two-phase	Air-0.15% Flowzan	252	1.5	0	8	4373
7	Two-phase	Air-0.15% Flowzan	285	1.5	0	8	5180
8	Two-phase	Air-0.15% Flowzan	315	1.5	0	8	5821
9	Two-phase	Air-0.15% Flowzan	222	2	0	8	4699
10	Two-phase	Air-0.15% Flowzan	252	2	0	8	4987
11	Two-phase	Air-0.15% Flowzan	285	2	0	8	5216
12	Two-phase	Air-0.15% Flowzan	315	2	0	8	5528